

UNIVERSITY OF OTTAWA

MASTERS THESIS

**Joint Angle-Based Skeleton Action
Recognition**

Author:

Nicolas FLEECE

Supervisor:

Dr. Robert LAGANIÈRE

*A thesis submitted in fulfillment of the requirements
for the degree of Master of Computer Science, Specialization in Applied AI
in the*

VIVA Research Lab
School of Electrical Engineering and Computer Science

UNIVERSITY OF OTTAWA

Abstract

Faculty of Engineering

School of Electrical Engineering and Computer Science

Master of Computer Science, Specialization in Applied AI

Joint Angle-Based Skeleton Action Recognition

by Nicolas FLEECE

Human action recognition is a difficult task and topic of discussion in the computer vision community. There are consistent breakthroughs by large research groups using sophisticated state-of-the-art computation hardware. These advancements allow for very accurate predictions on complex action recognition datasets that can be generalized to in-the-wild tasks. However, a key weakness is that in order to run these models, the computation required is significant.

We explore these models, as well as some models that utilize intermediate representations. These representations focus on the movement of the person throughout the frame, specifically the 'pose' data and translate this data into some intermediate representation that can be processed by compact models. We propose a novel intermediate representation utilizing only the angles of the joints of a person from one frame to another. This allows for the representation constructed to be completely invariant to the global position of the person in the frame, providing insights into how these small and very efficient representations and models can be used with good effectiveness.

“Sometimes I’ll start a sentence, and I don’t even know where it’s going. I just hope I find it along the way.”

Michael Scott

Acknowledgements

First and foremost, thank you to my supervisor Professor Robert Laganière, who answered my email when I was in search of a supervisor and has guided me through the process of writing and submitting this thesis. His knowledge was invaluable to me and I would not have been able to achieve this without him, providing me with endless opportunities that opened many doors that I would not have been able to open on my own.

Thank you to my family, without whom I would not be able to pursue this thesis and whose continued support helped push me to finish. Their both moral and financial support was crucial in my completion of my thesis, and helped me to push through the difficult parts.

Thank you to my partner, Monique, who helped through countless late nights of working, never complaining that I would always be running a model or writing paragraphs. Who read through pages of complex topics that she did not understand in order to correct my grammar mistakes, and spent late nights with our puppy Mabel while I was isolating myself trying to finish the final copy.

Working on my thesis during the pandemic has not been easy and there have been many points where I was questioning whether it was worth completing. I cannot name everyone who assisted me throughout the writing of this thesis and throughout my undergraduate degree prior to this. Herna Viktor, thank you for helping me with the application process to this masters, and for supporting me throughout my thesis with any questions I had, Lucia Moura, for helping me find a love for being a teaching assistant, and to all my professors who helped me develop my skills throughout my studies.

Contents

Abstract	i
Acknowledgements	iii
1 Introduction	1
1.1 Action Recognition	1
1.2 Applications	1
1.2.1 Ethical Issues	2
1.3 Challenges	4
1.4 Problem Definition	4
1.5 Contributions	5
1.6 Thesis Structure	5
2 Literature Review	6
2.1 Image Classification	6
2.2 Optical Flow	6
2.3 Convolutional Neural Networks	7
2.3.1 Structure	7
2.3.2 Classic Architectures	9
2.3.3 Modern Architectures	10
2.4 Recurrent Neural Networks	11
2.5 CNN Based Action Recognition Models	12
2.5.1 CNN + LSTM Models	13
2.5.2 3D CNN Models	16
2.6 Model Evolution	18
2.7 Datasets	19
2.8 Pose Detection	22

2.9	Pose-Based Action Recognition	23
2.9.1	Intermediate Representations	26
3	Methodology	32
3.1	Dataset Selection	32
3.2	Pose	32
3.2.1	Joint Angles	33
3.2.2	Joint Velocities	35
3.3	Novel Intermediate Representation	36
3.3.1	Representation Features	36
3.3.2	Representation Comparison	38
3.3.3	Temporal Adjustments	39
3.3.4	Model Architecture	41
4	Experimentation	44
4.1	Compute Resources	44
4.2	JHMDB Results	44
4.3	Failure Cases	47
4.4	Model Ablation Study	49
4.5	Model Comparison	54
5	Conclusion & Future Work	57
5.0.1	Future Work	58
Bibliography		59

List of Figures

2.1	A simple example of the optical flow field (c), resultant from the first and second frames (a) and (b). The goal being that the background is not in the optical flow field, only the movement of subjects in the frames are considered. In this case, the only movement from frame 1 and frame 2 is a slight upward movement in the bow.	7
2.2	Classical LeNet-5 architecture [9] containing convolutional, subsampling, and fully connected layers.	8
2.3	Example of how a kernel functions, being slid across the image and multiply by the kernel matrix.	9
2.4	VGG-16 [11] architecture, with 16 convolutional layers split into 5 blocks, each block being separated by pooling layers, ending with three dense layers which provide output.	10
2.5	The Residual Block utilized by the ResNet [12] model. The input is added to the output of the convolutional block, resulting in an output that has both the output of the convolutions as well as the original input, which can then be fed into further blocks.	11
2.6	Example of how an attention module will "focus" on the person performing the action, and filter out background information.	12
2.7	The general RNN structure, similar to the fully connected networks, except it contains a recurrence value. This recurrence is stored as a 'hidden state', which can be fed back into the network at the next time step.	13
2.8	An example structure of a simple CNN-LSTM based model, each individual frame being individually fed into the CNN, and then passed to a LSTM.	14

2.9 Action recognition structure for the LRCN model. [14]	15
2.10 Overview of the Beyond Short Snippets: Deep Networks for Video Classification model [18]	16
2.11 Deep LSTM module used in Beyond Short Snippets: Deep Networks for Video Classification [18]. The module consists of five separate LSTM models chained together	17
2.12 A portion of the original 3D-CNN action recognition model architecture proposed by 3D Convolutional Neural Networks for Human Action Recognition [20], containing a 3D convolution layer and 2x2 subsampling layer. The full architecture contains three convolutional layers, two subsampling layers and one fully connected layer.	18
2.13 The detailed inception submodule used in the I3D model [6].	19
2.14 The transformer encoder module utilized by the model proposed in An Image is Worth 16x16 Words: Transformers for Image Recognition at Scale [22].	20
2.15 Example feature outputs of how a transformer utilizes attention to focus on the main subject of a video in order to greater identify actions as shown in [22]	21
2.16 Simplified representation of the JHMDB pose that will be used later in this thesis. Notably the foot joints are missing as they are not reliably labelled and are not used by the model. The indexes correspond to JHMDB joint indexes as if the subject were facing the camera.	22
2.17 Example JHMDB [28] joint indices overlayed on a frame of the 'catch' action.	23
2.18 Examples from several JHMDB [28] classes with frames sampled throughout each video.	25
2.19 Illustration of P-CNN [33] feature construction. RGB & Optical Flow "Patches" are extracted around each joint, and sometimes containing multiple joints. These features are then passed through their respective CNN's. Note that in this figure only the RGB patches are shown.	26

2.20 A typical fused architecture. Each of the Pose, Optical Flow, and RGB Frames are passed through individual 3D-CNN's, the outputs are then concatenated to achieve a final output.	27
2.21 The chained architecture as shown in Chained Multi-stream Networks [34]. The model differentiates in that it has separate loss functions for each of Pose, Optical Flow, and RGB, which are chained together in a way that they can be individually optimized.	28
2.22 The illustration of the PoTion intermediate representation [35]. The input joint heatmaps are colored based on their time in the frame, and the frames are then concatenated to form the final movement of the joint throughout the video (the figure shows only one joint heatmap, the same process is followed for all other detected joints).	29
2.23 The main PA3D [37] model architecture, demonstrating the 1x1 convolutions used in order to construct the temporal cube, in this case on the right wrist.	30
2.24 The EHPI representation used in the Simple yet efficient real-time pose-based action recognition [38]. The x, y coordinates of each joint are mapped to the red & green values of a pixel, all joints are then stacked to form a column of joint positions in a frame. Each frame is then placed next to each other to form the 2D representation. In the case of this representation the 'B' value of RGB is always 0 since we only have x and y values.	31
2.25 The representation used by the Smaller, Faster, Better model [39], this is split into two representations. The cartesian coordinates of each joint are encoded into a 2 dimensional representation, not dissimilar to previously discussed models [38]. The JCD feature is a similar representation, but instead of x, y, and z coordinates, uses the distance between two joints.	31
3.1 Example of how joints are connected through bones in a typical pose representations.	33

3.2	Two examples of three joints interconnected with two bones, and how the angle can change from one frame to another.	34
3.3	An example skeleton with JHMDB indices in each of the joints. In addition, angles have been shown as if they are being calculated in a clockwise direction, resulting in connections such as 5-4-8 having the angle on the "outside" of the person.	35
3.4	Example of how the intermediate representation is constructed. At each frame, the angles of each joint are taken and added to a column, each column is then stacked next to one another to form a 2 dimensional image.	36
3.5	The finished intermediate representation, the top half contains the changes in joint angle from one frame to another (also referred to as "velocity"), and the bottom half contains the joint angles themselves. This is referred to as the "stacked" representation. In the representation, positive values are shown as red and negative values are shown as blue, with the higher values having more saturation.	37
3.6	Example of the rotation invariance of our representation. The angle represented is $A - B - C$, and is unaffected by a rotation around $C - D - E$, remaining at 45°	37
3.7	Comparison of our representation (b) compared to Simple yet efficient real-time pose-based action recognition [38] (a), showing a similar representation construction.	39
3.8	An example of the temporal adjustment on the golf action, skipping N frames between each image. As can be seen in (a), the movement is not as pronounced and the model may have difficulty determining the action because the velocity of the person is not very pronounced. When observing examples (c) and (d), the full action from one frame to another is much more clear and the deciphering of the intermediate representation would be easier as the movement is more pronounced.	40

3.9	Two examples of temporal adjustment to the stacked representation. In both cases, the representation skips N frames in each step, meaning with a $N = 1$ the representation will ignore every other frame, $N = 2$ every two frames, etc. As can be seen from the joint velocities, with example (b), the joint velocities are more intense and concentrated.	41
3.10	The basic model architecture used, very similar to that used in other models such as Potion [35], it is a simple 2 dimensional CNN that contains one fully connected layer at the end for classification.	41
3.11	Block diagram showing our intermediate representation from start to finish, including the pose estimation model that was not explored in this thesis.	43
4.1	Detailed F1 score results on the JHMDB dataset, averaged over the 3 testing splits. Black bars show the corresponding maximum & minimum values attained in one of the splits.	46
4.2	Three examples of the <i>Jump</i> class from the JHMDB dataset. The frames selected were four frames roughly evenly spaced out through the video.	47
4.3	Three examples of the <i>Golf</i> class from the JHMDB dataset. The frames selected were four frames roughly evenly spaced out through the video.	48
4.4	Detailed precision results on the JHMDB dataset, averaged over the 3 testing splits. Black bars show the corresponding maximum & minimum values attained in one of the splits.	49
4.5	Detailed recall results on the JHMDB dataset, averaged over the 3 testing splits. Black bars show the corresponding maximum & minimum values attained in one of the splits.	50
4.6	Confusion matrices for each of the 3 JHMDB splits.	51
4.7	An example of the catch action from the JHMDB dataset [28].	52
4.8	An example of the sit action from the JHMDB dataset [28].	52
4.9	Comparison between the walk (a) and climb stairs (b) actions from the JHMDB dataset [28] showing similar movements.	53
4.10	Detailed F1 score results on the JHMDB dataset using only the angle velocities from one frame to another.	54

4.11 Alternative intermediate representation format where angles and velocities are interlaced rather than stacked.	55
4.12 The split model architecture inspired by fusion models where the two different pose features are split and utilize independent CNN's.	55

List of Tables

2.1	Class counts for each class in the JHMDB dataset [28].	24
3.1	Example of how non-directional angle can result in incorrect rotation changes from one frame to another.	34
3.2	All Joint connections used in our intermediate representations. The joint angle that is focused on is centered on the B joint, with the two vectors $B \rightarrow A$ and $B \rightarrow C$ forming the angle used in the representation.	38
3.3	The detailed breakdown of the model architecture, split into 3 convolutional blocks and one dense layer used for classification. All convolutional layers utilize 3x3 convolutions, including a 1 pixel padding across all sides. The 2D max pooling utilized a 2x2 kernel, halving the size of the images after each convolutional block.	42
4.1	Results on all 3 splits of the JHMDB dataset utilizing only our novel approach.	45
4.2	Comparison of results using only angle velocities vs the stacked representation.	50
4.3	Comparison of results using only angles vs the stacked representation.	53
4.4	Comparison of results using the interlacing vs stacked representation.	54
4.5	Comparison of results using the split model and representation against the single CNN stacked representation.	56
4.6	Comparison of results using the final model compared to a shallower model using one less convolutional layer group, as well as a deeper model containing one additional convolutional layer group.	56

4.7 Model comparisons that do not contain very complex models and utilize mainly pose data. * - PA3D uses additional data in it's representation as well.	56
---	----

List of Abbreviations

AI	Artificial Intelligence
CIFAR	Canadian Institute For Advanced Research
CNN	Convolutional Neural Networks
EHPI	Encoded Human Pose Image
HMDB	Human Motion DataBase
I3D	Inflated 3D ConvNet
JCD	Joint Collection Distances
JHMDB	Joint-annotated Human Motion DataBase
LRCN	Long-term Recurrent Convolutional Networks
LSTM	Long Short-Term Memory
NLP	Natural Language Processing
PA3D	Pose-Action 3D Machine
P-CNN	Pose-based Convolutional Neural Network
PoTion	Pose MoTion
UCF	University of Central Florida

Chapter 1

Introduction

People interact with their environment in unique and nuanced ways, and throughout our lives, humans have learned to identify and categorize the different actions that we perform.

1.1 Action Recognition

For humans, the problem of human action recognition is rather simple. We use past experiences throughout childhood and adult life to be able to pick out the various ways a person moves, and translate that into a familiar action that we have seen before. Combine that with objects that a person may be interacting with, and humans are remarkably good at discerning what actions other humans are involved in. However, as is with most things in the domain of computer vision, this ability does not translate well into the realm of artificial intelligence. The slightly different ways that people may perform these tasks add a layer of complexity that is difficult for a model to overcome.

1.2 Applications

Security is perhaps the most obvious example of action recognition usage. Security personnel are constantly on the lookout for suspicious individuals that may be of concern, or who are performing illegal actions. This can be as simple as trying to find those who are shoplifting in stores, where the CCTV footage can be used live to find those who are actively stealing from stores. It could also be something more complex, such as security checkpoints in airports, where screening officers are

constantly watching for suspicious individuals. In this case, a system capable of analyzing the way every person acts and pointing out those who it sees as suspicious could greatly assist security personnel.

Health care is a slightly different, but nonetheless very interesting application of action recognition. A very large part of how action recognition can help those in the healthcare field is used in monitoring those who need around the clock care, primarily the elderly. If an elderly person chooses to live at home, the action recognition model may allow healthcare workers to, at a distance, manage many people and focus their attention on those who have been flagged by the model. This can often be done by very lightweight models [1].

Video summarization is perhaps not directly related to action recognition, but rather the study of action recognition is a very useful part of video summarization. If you must summarize a video where the main subjects tend to be humans, a large part of figuring out what is going on in the video is figuring out what action the person is performing, for example, for a summary to be something such as '*The person is fishing.*', the model must have some understanding of what fishing is. Similarly, if the main subject of the video is not a person, it may still be useful to know what those in the background are doing, for example '*A dog is sitting on a bench, there are people doing yoga in the background*', the model again must have an idea of what yoga is, and how a person performs said actions.

1.2.1 Ethical Issues

As with most applications of artificial intelligence, computer vision cannot be researched and discussed without taking into account the ethical issues that surround it. Given the rapid evolution of AI, it is imperative for researchers to remain cognizant of these ethical issues. In this section, we will focus particularly on how it may affect action recognition, touching on other areas of AI in general to further illustrate our points.

Privacy can become a concern in many areas, the healthcare example given previously in this chapter is one of the most obvious. With elderly people, often one of the draws to staying in their own homes is the privacy that it offers; if the action recognition model is to be used to ensure that they remain safe, it must come with

some removal of privacy. There is also a question of what happens to the data of a person who is using this kind of service. Given that data is likely sent to a server for processing, it prompts inquiry into the company's data retention policies, sharing practices, and whether the data will be used for training future models. These are all issues that often follow AI since the training of models requires such a massive amount of data, and in action recognition this can contain people who are not necessarily aware of their data being used in such ways.

Bias is one of the most common ethical issues in AI. In artificial intelligence, and computing in general, the principle of "garbage in, garbage out", is commonly used to illustrate that if the inputs into a model are not of high quality, the outputs will not be of high quality. This can often be the case in datasets where say a group of people are not accurately represented, and while the model itself is not discriminatory, it will follow the data it has been given. For example, airport security has been scrutinized in the past for singling out individuals of particular races or who look a particular way. This may mean that if a model is being constructed that searches for people who may be flagged later in security, the majority of positive flags that were screened further would be of this group of people. The resulting dataset that is constructed would be biased against this group of people, therefore resulting in a similarly-biased model. This type of issue has been shown in many different areas, another example being speech recognition models used by voice assistants not being able to recognize particular accents as they were not represented in the original dataset. These kinds of reasons are why it is crucial for researchers to be aware of and study their datasets when it comes to human data to avoid these biases and ensure that their data is well balanced.

Transparency is a rather difficult, and often nearly impossible problem to solve with modern AI models. Given the fact that these models at minimum have millions of parameters that all contribute to the complex calculations towards the output, deciphering exactly how they work and make their decisions is difficult. These models are often depicted as black boxes, where the only context we are given is what is input into the model and what the model outputs, and nothing in between. In the cases of something such as an airport security checkpoint, the model may mark a person as acting suspicious in a line of passengers. The model is not able to specifically

express what made the passenger appear suspicious, and it may even be incorrect in its assumptions. This means that the officer who is reviewing the flags set by the model has to make a decision that leads to one of two possible scenarios:

1. The model is correct, but cannot communicate its exact reasoning with the officer, the officer does not see what the model sees and a potential threat is ignored
2. The model is incorrect, but the officer thinks that he sees something, and a person who is not a threat is put through unnecessary security screening, and other potential threats may not be screened

1.3 Challenges

Human action recognition is a very difficult task that comes with many issues, some of which continue to be major challenges moving forward with very complex modern models.

Backgrounds are often not static in videos. Often they contain a lot of data that is ever changing and can contain other secondary subjects performing actions that may not be relevant to the subject that we are trying to determine the action of. While humans are very good at focusing on the person who is performing the action and ignoring things occurring in the background enough to not get confused, AI models do not have this inherent ability and often can get confused from background changes, and effectively must both identify the person and determine what action they are performing within the same model. This can be further worsened by any camera movement, resulting in both the subject moving throughout the frame as well as the background moving behind the subject.

1.4 Problem Definition

The problem of human action recognition is defined as taking a video of a person performing a particular action, and passing it through a model to determine the

specified action the person is performing. Pose-based action recognition is the problem of performing this detection primarily using the skeleton data of the people in the frame.

1.5 Contributions

The primary contribution that this thesis provides is a novel intermediate representation that can be used in tandem with a simple CNN for use in the problem of human action recognition. This representation is designed such that it is invariant to: the global position of the person, the distance between the camera and the person, and any background information. This representation only utilizes the skeleton data of the person, specifically the joint angles of a person and how they change from one frame to another.

1.6 Thesis Structure

This thesis will begin by exploring the research relevant to action recognition in chapter 2. Next, a novel representation is proposed in chapter 3, and the experiments and their results are detailed in chapter 4. Finally, the conclusions and recommendations for future work are presented in chapter 5.

Chapter 2

Literature Review

2.1 Image Classification

Image classification is one of the precursor problems to action recognition. Without the ability to classify individual images, the ability to classify videos, which functionally are a list of individual images, would never have been researched as nearly every technique for action recognition can be tracked from some form of image classification task.

An example of this task is the CIFAR dataset [2], where the goal is to simply classify relatively low resolution images into either 10 or 100 classes, depending on the version of the dataset. Some simple models such as EfficientNet [3] are able to achieve above 90% accuracy while providing a model that is able to be trained efficiently and evaluate images quickly. In addition, some sophisticated models are capable of achieving scores above 95% [4] [5]. The popularization of image classification led to the popularization of CNN's which are also actively used in action recognition, and particularly popular in intermediate representation models that will be discussed in section 2.9.1.

2.2 Optical Flow

Optical Flow is often taken for granted in models that utilize it, however it can be computed in several different ways. An example of a model that leverages optical flow is the Two-Stream Inflated 3D ConvNets model [6] which will be discussed later in this chapter in section 2.5.2. The specific details of optical flow are very complex and ultimately outside the scope of this thesis, the idea that provides performance

improvements is that optical flow represents the movement of a person from one frame to another and eliminating background information which does not move. This idea is demonstrated in figure 2.1.



FIGURE 2.1: A simple example of the optical flow field (c), resultant from the first and second frames (a) and (b). The goal being that the background is not in the optical flow field, only the movement of subjects in the frames are considered. In this case, the only movement from frame 1 and frame 2 is a slight upward movement in the bow.

2.3 Convolutional Neural Networks

Convolutional Neural Networks are a key part of both this thesis and the larger domain of computer vision. When these models were developed, computer vision took a large step forward in the domain of image processing, and is still being developed by modern models in order to extract further performance [8].

2.3.1 Structure

The classic structure of a convolutional neural network can be studied through one of the first recognizable architectures; LeNet-5 [9], as shown in figure 2.2. This architecture is broken into a few key layers that are common in classical CNN's:

- Convolutions
- Subsampling
- Flatten
- Fully Connected

The **convolutions** are the key part of how convolutional neural networks function, and they function using a **kernel**. This kernel is built as an $N \times N$ matrix of

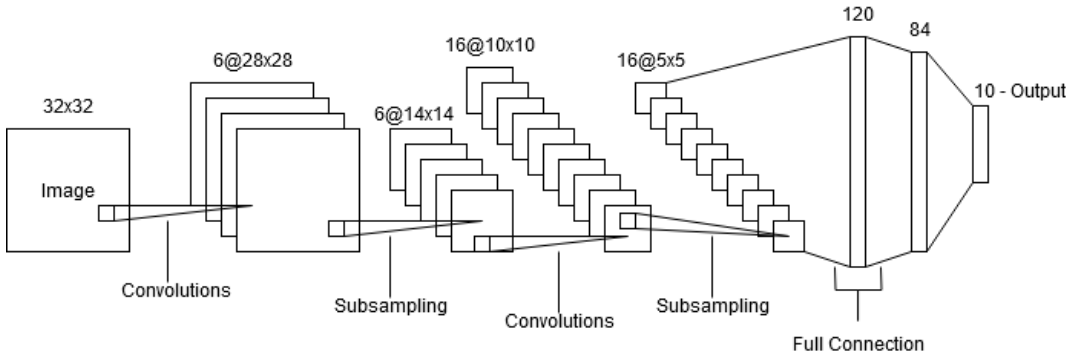


FIGURE 2.2: Classical LeNet-5 architecture [9] containing convolutional, subsampling, and fully connected layers.

randomly initialized values. The matrix is then ‘slid’ across the entire image, and the values that the kernel ‘sits on top’ of are multiplied by the kernel values and then summed to produce an output cell in the output image. An example of a 4×4 greyscale image and 2×2 kernel is shown in figure 2.3. In addition to this process, sometimes the edges of images are ‘padded’ with zeroes in order to avoid the reduction in image size when a kernel reaches the edge of an image. This kernel can also be expanded to 3 dimensions in order to be utilized on video data rather than image data. This functionally works the same as 2-dimensional convolutions, sliding in three directions instead of two, however it results in much larger kernels that take up significantly larger portions of memory. This is because the back-propogation data must be then stored for 27 kernel data points rather than 9 (in the case of a 3×3 convolution).

The **subsampling** (also commonly referred to as **pooling**) layers work in a similar way to convolutions, however instead of being trained, they are simply a standardized filter designed to down sample the feature maps exported by convolutional layers. This can be done through a few methods, average (as is used in LeNet) or max pooling are the most implementations. They simply take either the maximum or average value of the values covered by the subsampling kernel. The **flatten** layer simply transforms the outputs of the convolutional layers from shape $A \times B \times C$ to a one-dimensional vector of length $A * B * C$. This can then be passed through the **fully connected** layers, which are identical to those used in traditional fully-connected neural networks.

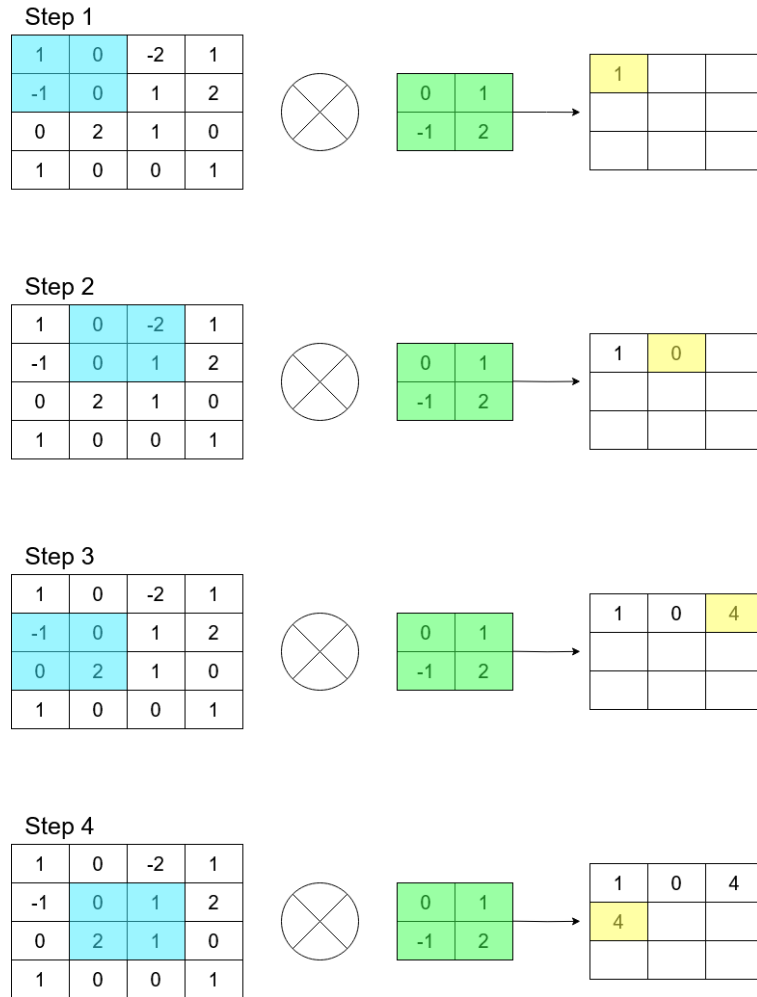


FIGURE 2.3: Example of how a kernel functions, being slid across the image and multiply by the kernel matrix.

2.3.2 Classic Architectures

AlexNet [10] is another common CNN architecture not dissimilar to the LeNet architecture [9] shown previously in this chapter. AlexNet provided two main contributions over the LeNet architecture. First, it provides a new method of training models on GPU, which involves splitting the parts of the model to be trained separately on different GPU's which can then be combined at the end, which allowed more overall GPU memory to be utilized when training the model. Second, it provides a much deeper CNN architecture, where the LeNet architecture contains only 2 convolutional layers, the AlexNet architecture contains 5 total convolutional layers, three of which are stacked one after another after the second max pool layer. When it was introduced, AlexNet was the state-of-the-art CNN for image classification and opened new doors with efficient multi-gpu trained models.

VGG-16 [11] is another deep convolutional neural network model, again similar to those described previously in this section, however as AlexNet [10] built complexity on top of LeNet [9], VGG-16 seeks to do the same over AlexNet. The '16' part of VGG-16 refers to the number of convolutional layers, which is much more than the 5 present in AlexNet. While this added complexity is important, VGG-16 also focuses on keeping the individual parts simple, for each of their convolutional layers, the kernel is 3x3 with stride 1, and for each of the pooling layers, they utilize a 2x2 filter with stride 2. These convolutions are split into five different 'blocks' shown in figure 2.4, which are separated by these pooling layers, ending with the same structure of dense layers present in AlexNet.

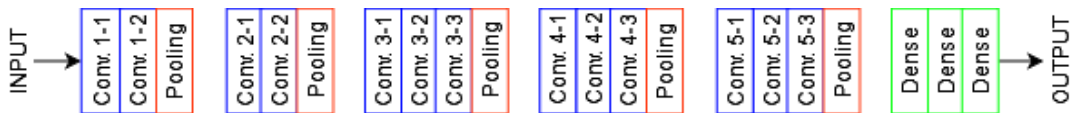


FIGURE 2.4: VGG-16 [11] architecture, with 16 convolutional layers split into 5 blocks, each block being separated by pooling layers, ending with three dense layers which provide output.

2.3.3 Modern Architectures

ResNet [12] deviates from this base CNN structure, aiming to improve on how these complex CNN's process data. With the evolution of CNN's naturally becoming more complex, the simplest approach was to add more convolutional layers (as can be seen from the transition from simple networks such as AlexNet [10] to more complex networks such as VGG-16 [11]). ResNet takes issue with this strategy, noting the problems of vanishing/exploding gradients becoming more prevalent and preventing the models from converging on proper solutions even if there is sufficient complexity present. They aim to mitigate this issue via a simple "Residual block" shown in figure 2.5.

The function of the residual block is to make the model fundamentally easier to train. By separating the input into two parts $F(x)$ and x , the input to the next block will not have to rely on solely the outputs of the convolutional layer ($F(x)$), rather it can use the original input to the previous block x as well. This means that further convolutional blocks do not need to rely on the accuracy of $F(x)$, meaning that each block can focus on fitting individual patterns. This results in very complex networks

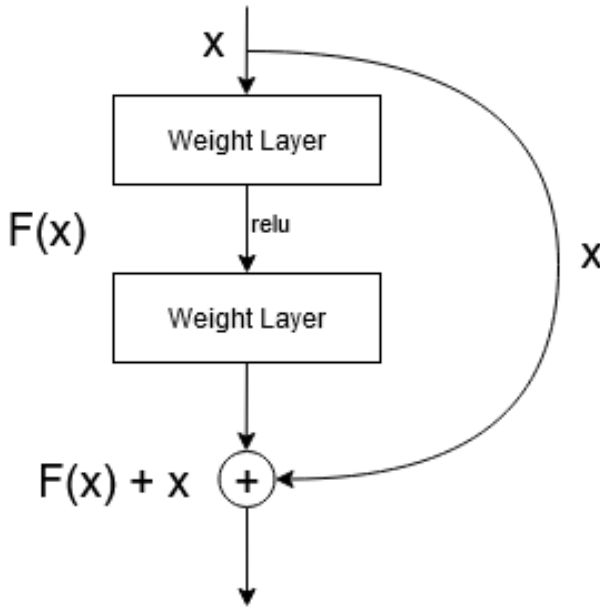


FIGURE 2.5: The Residual Block utilized by the ResNet [12] model. The input is added to the output of the convolutional block, resulting in an output that has both the output of the convolutions as well as the original input, which can then be fed into further blocks.

that can still reliably find simple patterns, contrary to previous models where these simple details are lost to many stacked convolutions. This same method is employed in classic feed-forward neural networks as well using "shortcut connections", which functionally work in a very similar way to the residual blocks and has also proven to give performance increases.

Residual Attention Network for Image Classification [13] was another advanced technique to build off the existing CNN architecture that ResNet provided. This model aims to utilize attention modules, as shown in figure 2.6, which help the model to highlight points in the image that are more relevant to the image, and filter out background data. Again, building upon previous works, this model utilized the residual blocks used in ResNet [12], making it so that the model is able to be very deep and very complex without falling prone to vanishing/exploding gradients as easily.

2.4 Recurrent Neural Networks

A Recurrent Neural Network (RNN) are a variation on the classic fully connected layer structure. These networks through a 'recurrence' connection that connects the



FIGURE 2.6: Example of how an attention module will "focus" on the person performing the action, and filter out background information.

output layer back into a previous layer. This is shown in detail in figure 2.7. This recurrence is stored as a 'hidden state', meaning that we can chain inputs from one example to another.

The primary application for these kinds of networks is utilizing them for time series analysis. This is because for each step of the time series, we get a hidden state that we can then pass to the next step of the time series. This therefore means that the model is capable of analyzing the time series one step at a time while outputting at each corresponding step. This ability to process any amount of data also allows us to utilize it for video analysis because the any number of frames can be processed one at a time from the video.

A Long Short Term Memory Network (LSTM) is a variation of the RNN model. This network works in a very similar way, being constructed in a way that there is a 'hidden state' that can be passed to the next time step, however the previous hidden state and input data are combined with the recurrence value and create a new hidden state. The goal of this being that the model does not have a bias towards recent data, but instead retains some information from very early time steps.

2.5 CNN Based Action Recognition Models

Naturally, the first approach to feeding video data into models is to process the raw RGB frames. This technique is derived from image classification tasks, where

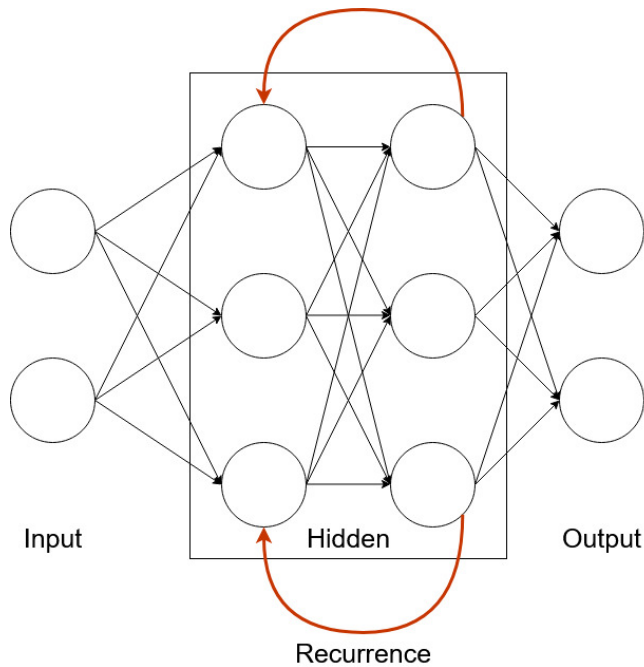


FIGURE 2.7: The general RNN structure, similar to the fully connected networks, except it contains a recurrence value. This recurrence is stored as a ‘hidden state’, which can be fed back into the network at the next time step.

lightweight and relatively simple CNN’s have been shown to have good performance when classifying single images. The logic would then follow that these types of models may be able to classify videos with fair accuracy, however they must be modified, which will be described further in this chapter.

2.5.1 CNN + LSTM Models

In very classic models, utilizing existing CNN architectures is a very simple process. The individual frames are passed through the CNN, producing a feature map for each frame. These feature maps are then flattened and passed into a RNN which produces an output.

Figure 2.8 shows the typical modern structure for this solution. After the features are extracted from each of the 2 dimensional CNN, they are passed through a LSTM. The goal of this LSTM module is to carry features from one frame to another and add some temporal element.

The advantages of this model are that it is very lightweight and all of the individual parts are already well studied and efficient. This also means that the models are very lightweight, and relatively simple in comparison to more complex techniques.

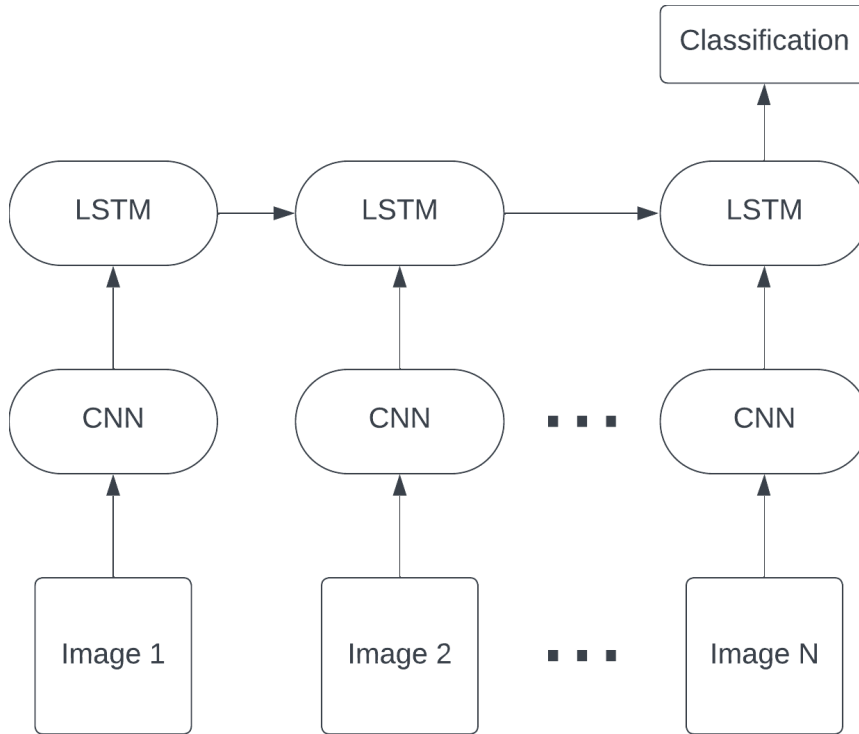


FIGURE 2.8: An example structure of a simple CNN-LSTM based model, each individual frame being individually fed into the CNN, and then passed to a LSTM.

The disadvantages of the model are also rooted in its simplicity. The result of processing each image independently means that the interactions between frames is not very well represented. While the model is able to represent individual frame features very well, due to the fact that the feature maps are passed through the LSTM, classes that require specific movement from one frame to another are difficult to learn using this structure. Constructing these individual feature maps can also fall victim to background interference, meaning that a movement in the camera, or change in background could impact in a way that detracts from the main subject of the action more with this model than the other approaches discussed later in this chapter.

Long-term Recurrent Convolutional Networks (LRCN) [14], is a model constructed using this methodology. In the paper, they use the notation that each frame, x_i , is fed into the CNN in order to construct a fixed-length feature representation, $\phi_v(x_i)$. This is then passed into the recurrent sequence learning model. This is where the model differs from the previous example provided. In the LRCN model, the LSTM outputs at each frame are averaged to get the output class, rather than taking

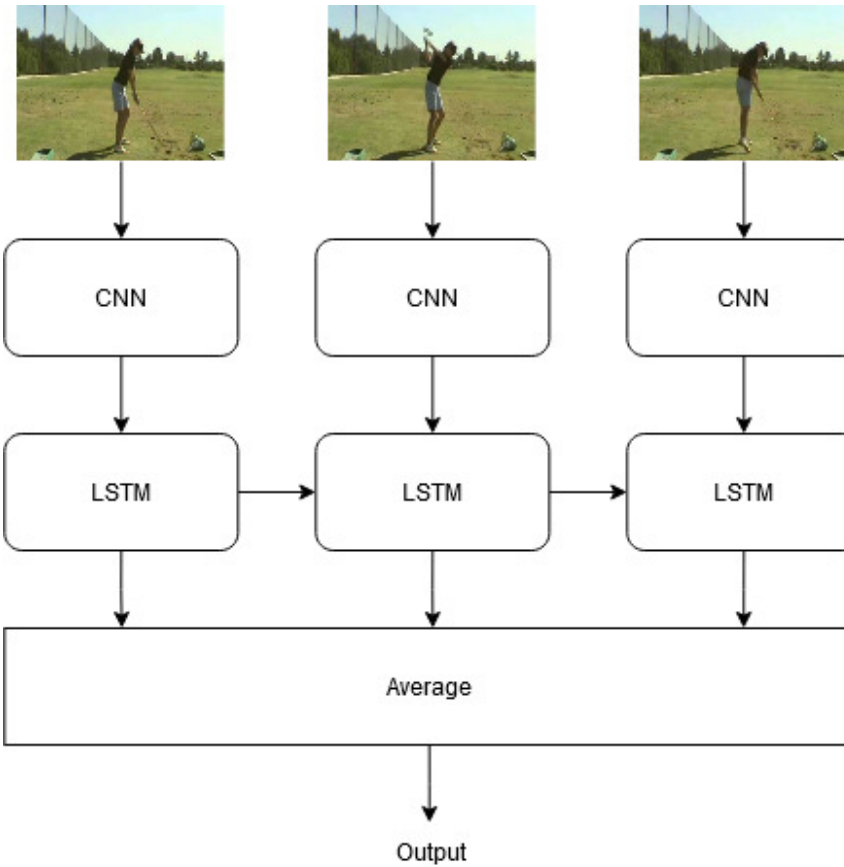


FIGURE 2.9: Action recognition structure for the LRCN model. [14]

the last output. This removes any bias the model may have towards the later frames in long videos. In addition to RGB frames, this model uses the optical flow feature, which easily adapts to this structure, replacing the RGB frames in figure 2.9. The LSTM structure is taken from **Learning to Execute** [15], which is a structure devised from the original LSTM model. The CNN, represented in the paper as ϕ , is described as a hybrid of the CaffeNet [16] (a variant of the AlexNet [10] model discussed in section 2.3.2) and the Zeiler and Fergus [17] models, which has been pre-trained on a large dataset.

Beyond Short Snippets: Deep Networks for Video Classification [18], is another approach to this structure, which explores a more complex deep-LSTM based module, as well as more classical feature pooling. The block diagram of this model shown in figure 2.10. Similarly to the previously discussed model, Long-term Recurrent Convolutional Networks [14], the model utilizes a combination of two popular CNN models, AlexNet [10] and GoogLeNet [19]. The paper did explore many more

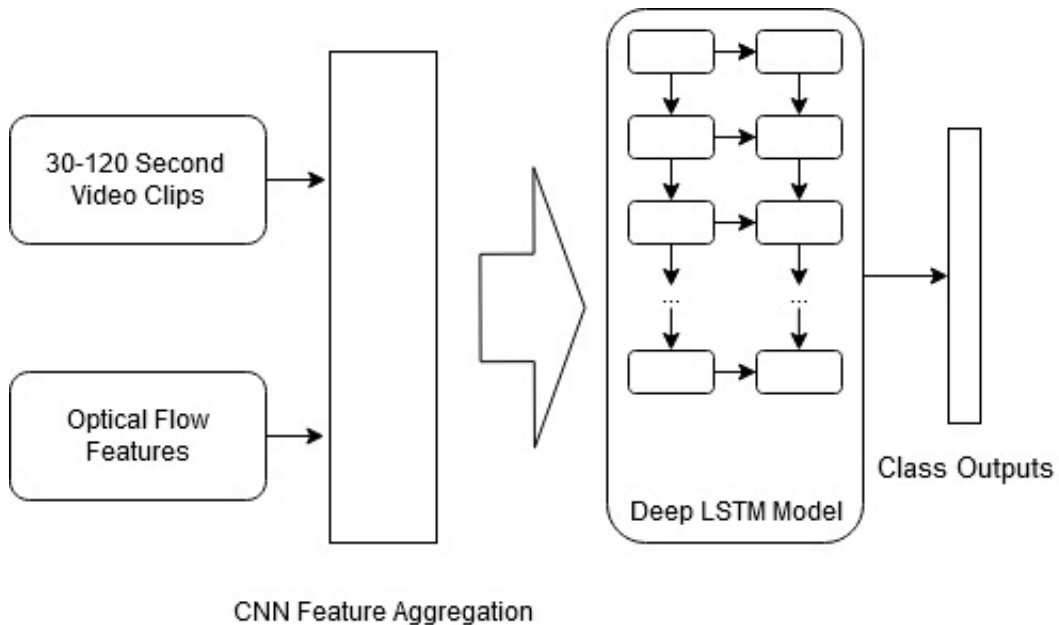


FIGURE 2.10: Overview of the Beyond Short Snippets: Deep Networks for Video Classification model [18]

classical feature pooling architectures, and were proven to have good results, however these techniques were outperformed by the deep LSTM model. The paper utilized a deep LSTM architecture for the feature aggregation step which further adds to its complexity, moving it above the CNN-LSTM architectures described previously. In this deep-LSTM module, the outputs of each frame are passed into a LSTM module as in the previous model, but the outputs are then passed through 4 more stacked layers of LSTM's, after reaching softmax layers which are averaged to get an output. These 4 additional layers of LSTM's mean it is more able to infer data moving from one frame to another. This model additionally explored the uses of optical flow and found that it adds a great deal to the accuracy of the model.

2.5.2 3D CNN Models

When considering how to handle videos without the LSTM component, the one of the first approaches that was developed is to utilize 3 dimensional CNN kernels. The function of these kernels when it relates to action recognition is that they allow for the model to easily encode local temporal data using the third kernel dimension. The primary issue with these models is that they contain many more parameters

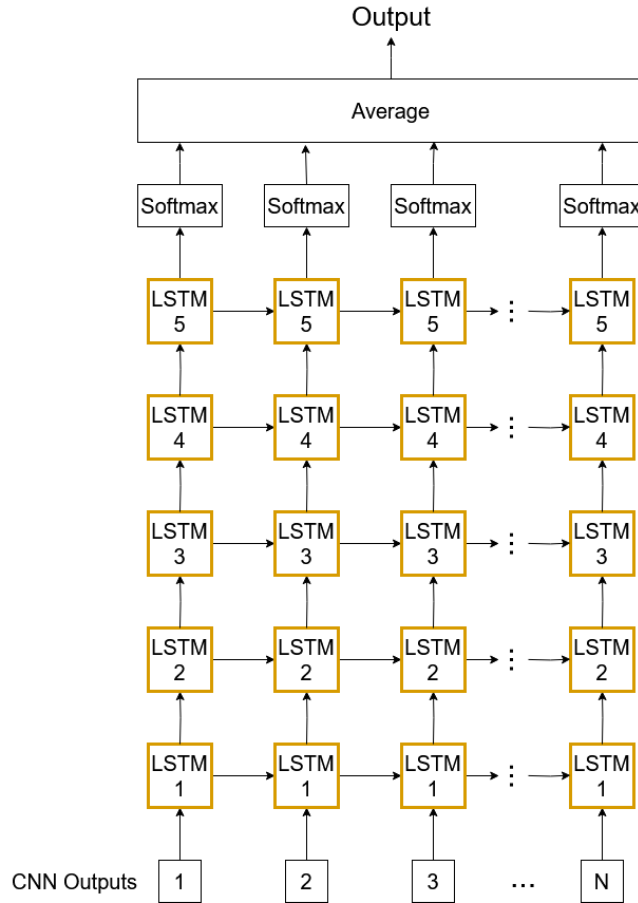


FIGURE 2.11: Deep LSTM module used in Beyond Short Snippets: Deep Networks for Video Classification [18]. The module consists of five separate LSTM models chained together

over the 2 dimensional CNN models, meaning that they take longer to train and require more computing power as compared to the lightweight counterparts.

3D Convolutional Neural Networks for Human Action Recognition [20] was one of the original papers that proposed this model for the purposes of action recognition, and the greater topic of 3 dimensional convolutions. The general architecture of the model is shown in figure 2.12, and is extremely similar to that of 2 dimensional CNNs, with convolutional layers which are followed by subsampling layers.

The primary difference with this original architecture compared to 2D CNN's as we know them today is that it used rather large $7 \times 7 \times 3$ convolutions, as compared to the typical 3×3 convolutions used in classical 2D CNN's. **Learning Spatiotemporal Features with 3D Convolutional Networks** [21] is a slightly more modern architecture that was proposed. They explore in great detail the effects of these sizes of convolutions and find that this size of convolutions are more effective than the

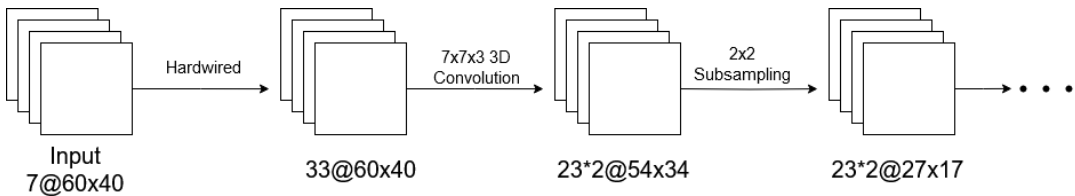


FIGURE 2.12: A portion of the original 3D-CNN action recognition model architecture proposed by **3D Convolutional Neural Networks for Human Action Recognition** [20], containing a 3D convolution layer and 2x2 subsampling layer. The full architecture contains three convolutional layers, two subsampling layers and one fully connected layer.

previous methods and sizes.

Two-Stream Inflated 3D ConvNets, commonly referred to as I3D [6], is a modern variation on 3D CNN based networks. Similar to the previously discussed model [20], this model explores the viability of taking techniques used in 2D CNN models and applying them to 3D. However it takes a much more direct approach, stating that they take the square filters of size $N \times N$ and convert them simply to 3D filters with dimensions $N \times N \times N$, a process they describe as *inflating* the convolutions. In addition to this, they utilize a repeated inception submodule shown in figure 2.13. This inflation of convolutions allows for I3D to replicate successful 2D CNN's in their structure and apply them to video with little modifications.

2.6 Model Evolution

Transformers for Image Recognition at Scale [22], extends beyond CNN's to explore transformer networks. While transformer networks are very easily applied to natural language processing tasks, it is not as easily applied to video and in particular action recognition. As depicted in figure 2.14, the model utilizes a transformer encoder architecture in order to learn features that are useful for action recognition. The goal of this being to leverage previously well studied NLP studies that indicate the attention features of transformers are useful for focusing on the relevant data. Figure 2.15 shows this effect, the goal of this being to mitigate the challenges of handling background data interference as previously described in section 1.3. This logic is then further expanded upon in many future models to extend this functionality,

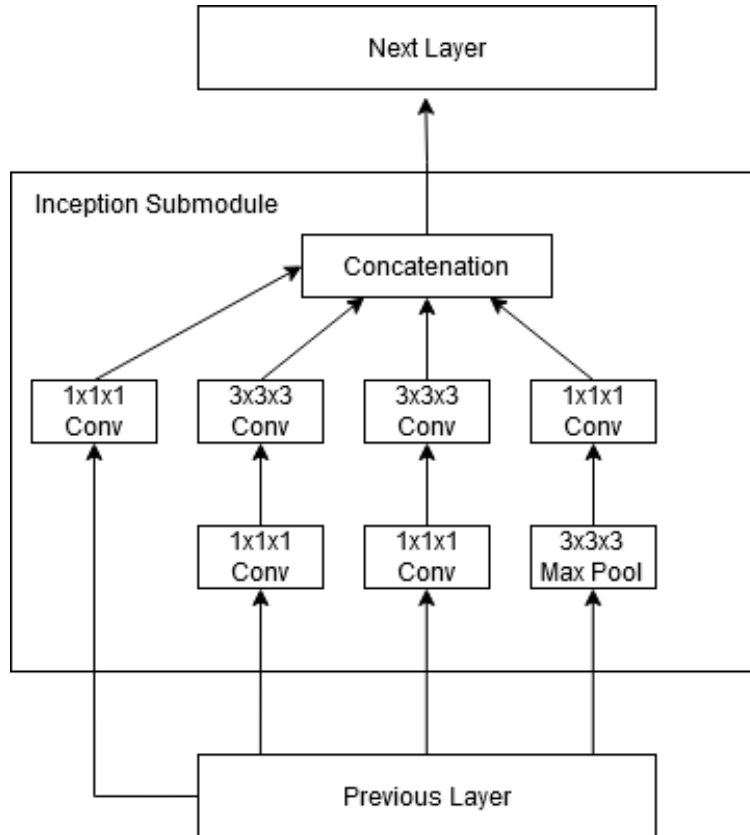


FIGURE 2.13: The detailed inception submodule used in the I3D model [6].

such as **Multiview Transformers for Video Recognition** [23] which explores using multiple separate encoders to explore multiple views.

2.7 Datasets

There are many action recognition datasets, some of which fit more specific use cases, and others which are more general and tailor to more in-the-wild data (an uncontrolled environment outside of pre-defined datasets, this data often has many challenges not encountered in pre-defined datasets). For example the Charades dataset [24] focuses more on actions of people indoors and their interactions, whereas other datasets such as THUMOS [25] focus on many in-the-wild videos, where the location of the person can be different.

The Kinetics Human Action Video Dataset [26] is one of the primary in-the-wild action recognition datasets that are reported on by modern models. The primary advantage of this dataset over others that were published around the same time such as

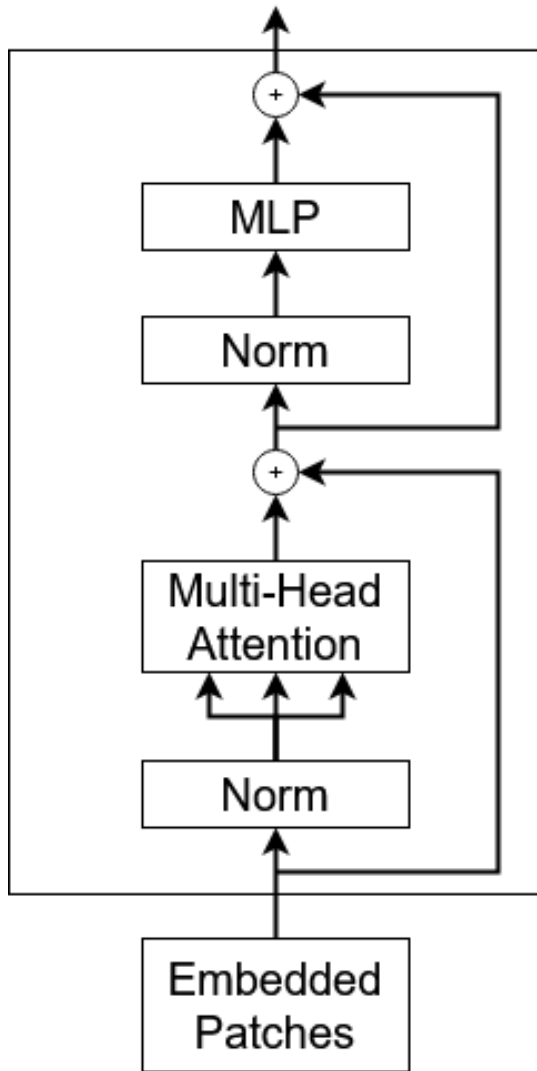


FIGURE 2.14: The transformer encoder module utilized by the model proposed in **An Image is Worth 16x16 Words: Transformers for Image Recognition at Scale** [22].

the UCF-101 dataset [27] is that as opposed to UCF's 101 classes and approximately 13,000 clips, the original kinetics dataset contained 400 classes and approximately 300,000 total clips which is magnitudes greater than other datasets of this type. This dataset was also updated in 2020 to include 700 classes and over 600,000 clips. The extremely large amount of these clips, as well as containing all of; singular person actions (eg. headbanging, stretching), person-person actions (eg. handshake, tickling), and person-object actions (eg. riding a bike) among others creates a dataset that is difficult for a model to determine what action is being performed.

Joint-annotated Human Motion DataBase (JHMDB) [28] is the primary dataset that will be used in this thesis. The JHMDB paper does not actually propose an



FIGURE 2.15: Example feature outputs of how a transformer utilizes attention to focus on the main subject of a video in order to greater identify actions as shown in [22]

entirely new dataset, rather it proposes a subset of the Human Motion DataBase (HMDB) dataset [29], with the addition of several features, primarily annotated poses (hence the Joint-annotated addition to the original dataset name). While the dataset does offer more than only annotated poses, the main appeal of the dataset when considering the method used in this thesis is that they are manually annotated and adjusted poses to ensure that they are correct, meaning that the model can be independently be evaluated without having to consider the accuracy of the pose estimation model. Additionally, the dataset has been pruned such that the actions within the dataset only contain single person interactions, that lends itself very well to pose-based models, as generally only pose can be considered and the model can provide accurate results. Both of these features result in the dataset being highly popular with 2D-pose based models, and in particular models that create intermediate representations with these poses, as the data that is extracted from pose is both accurate and relevant to the action.

The JHMDB dataset contains a total of 928 video clips separated into 21 classes. The breakdown of class examples is shown in table 2.1. These examples are split into 3 different splits, one of which is used for testing and the other two for training, this is further explored in section 4. Each of these videos is approximately 40 frames in length. Typically most of the person is in the frame in these videos, and one person is the focus of the action. Some examples of frames in videos are shown in figure 2.18.

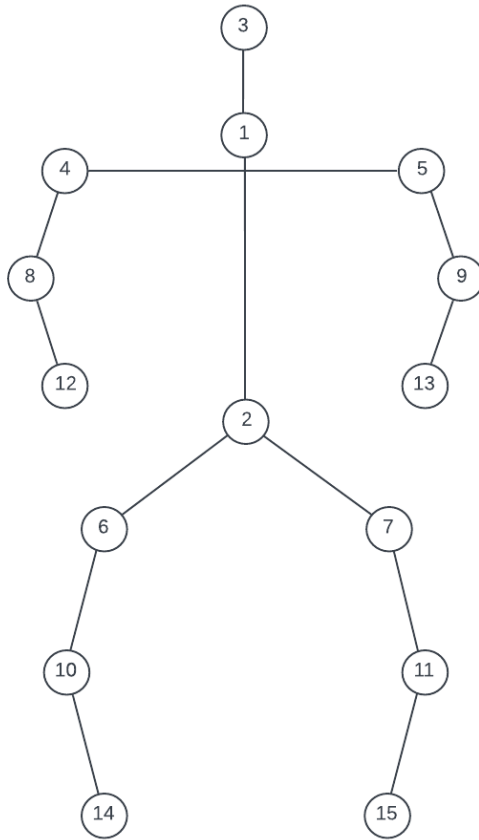


FIGURE 2.16: Simplified representation of the JHMDB pose that will be used later in this thesis. Notably the foot joints are missing as they are not reliably labelled and are not used by the model. The indexes correspond to JHMDB joint indexes as if the subject were facing the camera.

2.8 Pose Detection

Throughout the majority of this thesis, and in some pose-based papers, the concept that there is some form of extracted pose from any given RGB frame is assumed to be accurate and complete. However the extracting of these pose features, especially in the wild, is a difficult task in and of itself. This means that when considering pose-based action recognition models (as will be done further in section 2.9) the accuracy of these techniques must be taken into account. Without an accurate pose model, it is impossible for these pose-based action recognition models to perform with any level of accuracy. It is also worth noting is that some training data can have manually annotated pose data, an example being the previously discussed JHMDB dataset [28]. A very common model utilized by pose-based models is **OpenPose** [30] which is capable of detecting the poses of many people within the frame. Some



FIGURE 2.17: Example JHMDB [28] joint indices overlayed on a frame of the 'catch' action.

models utilize the heatmaps of potential joint positions instead of the standard pose information, which can also be easily generated by OpenPose. This is done through a modern technique using large CNN's and leveraging Part Affinity Fields, it also allows for very fast real-time pose estimation.

There are many other pose estimation models, as it is in itself a problem in the domain of computer vision that is constantly evolving and is ultimately outside the scope of this thesis. These can range from transformer based models such as ViTPose [31] designed to maximize dataset metrics, to the very lightweight models such as MoveNet developed by TensorFlow [32], developed for the purposes of real-time pose detection through mobile devices.

2.9 Pose-Based Action Recognition

Pose-based action recognition models have been well studied, and have been one of the popular forms of action recognition model as people typically determine actions by examining how a person is moving. This is because by focusing on the pose

Class	Number of Examples
<i>brushhair</i>	41
<i>catch</i>	48
<i>clap</i>	44
<i>climbstairs</i>	40
<i>golf</i>	42
<i>jump</i>	39
<i>kickball</i>	36
<i>pick</i>	40
<i>pour</i>	55
<i>pullup</i>	55
<i>push</i>	42
<i>run</i>	40
<i>shootball</i>	40
<i>shootbow</i>	53
<i>shootgun</i>	55
<i>sit</i>	39
<i>stand</i>	36
<i>swingbaseball</i>	54
<i>throw</i>	46
<i>walk</i>	41
<i>wave</i>	42

TABLE 2.1: Class counts for each class in the JHMDB dataset [28].

(sometimes referred to as the skeleton) of the person, you are able to effectively mitigate the background effects that were discussed in section 1.3. This means that typically more lightweight models can be used as they are able to be pointed more towards the main subject rather than filtering out background data. Of course this method also comes with challenges, notably that in testing in the wild, there must be effectively two models, one to extract the pose from the person(s) in the frame, and one to process this pose data and export an action. This can introduce another point of failure, but as discussed in section 2.8, 2D pose detection has been consistently improving to the point that high quality pose data from fast models is becoming the norm.

Pose-Based CNN Features for Action Recognition (P-CNN) [33] is a model that utilizes this pose. They use patches of the RGB frames centered on the various joints that have been detected, this is shown more in detail in figure 2.19. While this model does improve on typical models by using pose data, it does still struggle from the fact that it uses the raw RGB frame data, resulting in a model that is larger than



FIGURE 2.18: Examples from several JHMDB [28] classes with frames sampled throughout each video.

would be desired.

Fusion-based architectures have had success in combining techniques used by basic 3D-CNN's, as seen in the I3D model [6], which as previously discussed in section 2.5.2 utilizes the RGB Frames & Optical Flow in order to predict actions. Pose can be added to this architecture as shown in figure 2.20, where the pose data is added using some additional representation, the simple being the joint heatmaps exported from a previous model, and becoming more complex with intermediate representations that will be further discussed in section 2.9.1. **Chained Multi-stream Networks Exploiting Pose, Motion, and Appearance for Action Classification and Detection** [34] is an addition to this type of model, where instead of the classic fused architecture, the model has individual loss functions added to each of the outputs,

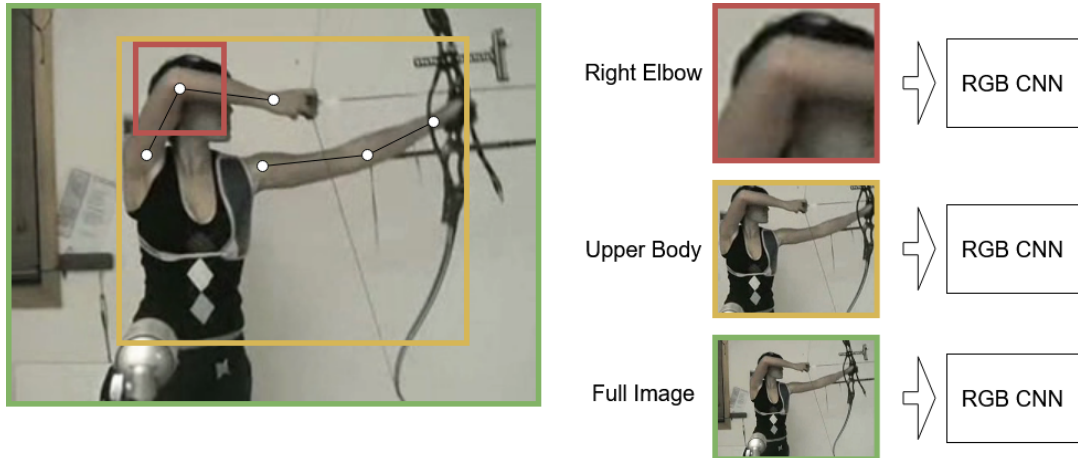


FIGURE 2.19: Illustration of P-CNN [33] feature construction. RGB & Optical Flow "Patches" are extracted around each joint, and sometimes containing multiple joints. These features are then passed through their respective CNN's. Note that in this figure only the RGB patches are shown.

increasing performance while not adding significant additional complexity to the model.

2.9.1 Intermediate Representations

Intermediate representations are the basis for what will be discussed in later sections of this thesis. Intermediate representations aim to reduce the pose data that has been extracted into simpler and more processable formats. This is generally done with the aim of using a more lightweight model (typically a 2D CNN rather than 3D) that requires significantly less computing power. Of course, this kind of pre-processing comes with issues, notably that by converting the model into an intermediate representation, some data will inevitably be lost during the transition, so the problem definition shifts slightly to creating an intermediate representation that both allows for a lightweight model to be effectively trained on it and for the smallest amount of data to be lost in the transition.

Pose MoTion Representation for Action Recognition (PoTion) [35] proposed one of these intermediate representations, however they did it in a way that was unique in that they only considered the joint positions rather than the skeletons themselves. Namely, the model utilizes the joint positions of a person throughout each frame of video to construct 2 dimensional images that reflect the movement of each of these joints. This is done by stacking each joint heatmap onto one image,

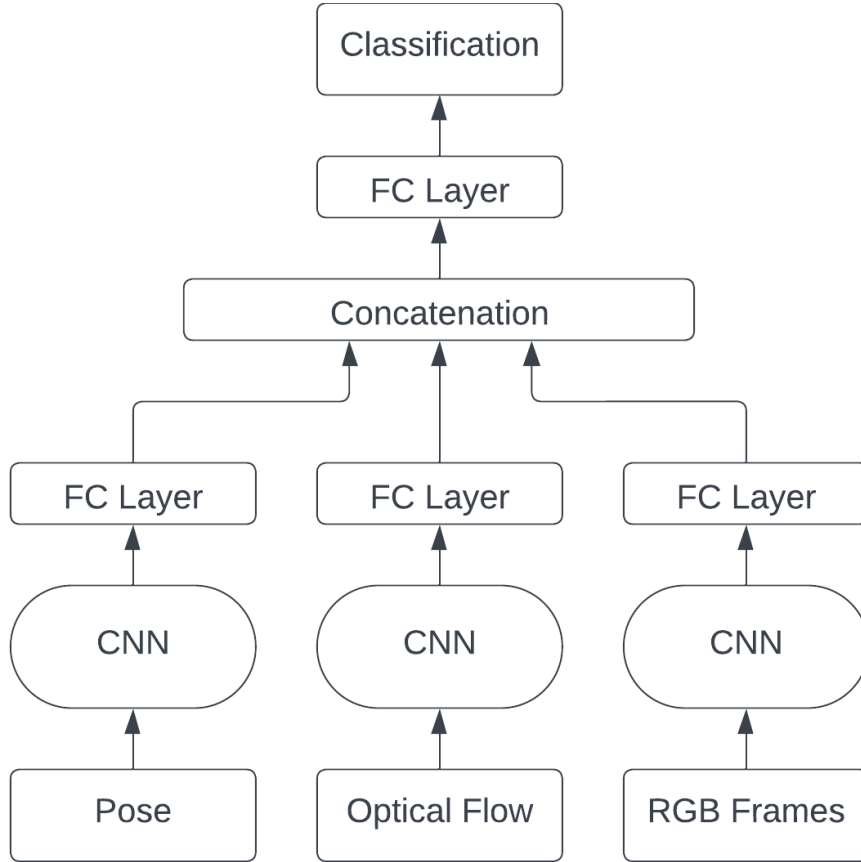


FIGURE 2.20: A typical fused architecture. Each of the Pose, Optical Flow, and RGB Frames are passed through individual 3D-CNN's, the outputs are then concatenated to achieve a final output.

and colorize them according to the point in time the frame is extracted. The overall representation construction is shown in figure 2.22, and shows how after the colourization is performed, the heatmap images are then stacked together. These stacked images can then be passed into a simple 2D CNN, which can be quickly and efficiently trained and performs rather well. In the paper they also explore adding this implementation as another input to the I3D [6] model in conjunction with the optical flow and rgb frames, which it showed to offer an increase in performance to the existing model. **Pose and Joint-Aware Action Recognition** [36] is a slight improvement on this model structure, they utilize a similar colorization scheme. Instead of feeding all of the joints into the model, they developed a joint-motion re-weighting network (denoted in the paper as JMRN), which allowed for the model to easily find the dependencies between joints. This joint selection procedure allowed for the model to offer improved performance over the original PoTion model.

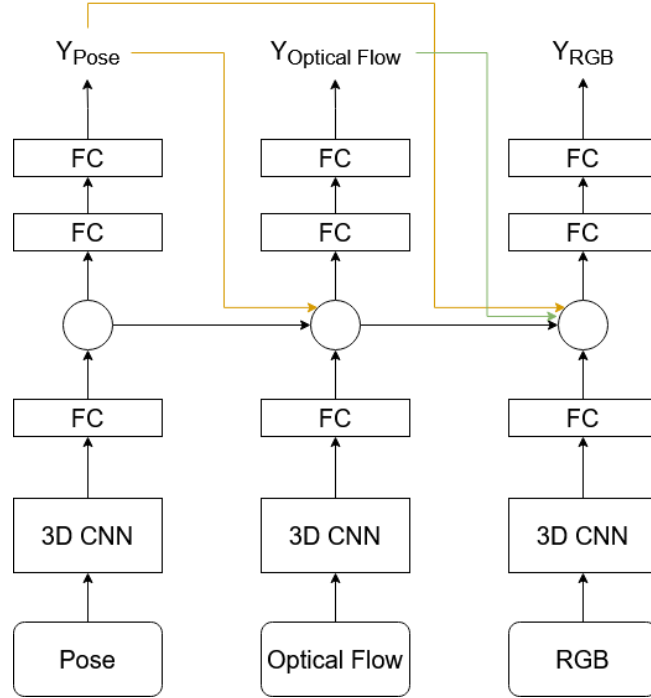


FIGURE 2.21: The chained architecture as shown in Chained Multi-stream Netowrks [34]. The model differentiates in that it has separate loss functions for each of Pose, Optical Flow, and RGB, which are chained together in a way that they can be individually optimized.

Pose-Action 3D Machine for Video Recognition (PA3D) [37] takes a similar approach to the PoTion model, but flavours it slightly differently. Similar to PoTion model, it leverages joint heatmaps similar to that exported from the OpenPose pose detection model, however it does not colorize the joints and aim to insert them into one image. A part of the model known as the Temporal Pose Convolution, shown in figure 2.23 is a core part of how the model functions. This is done through $1 \times 1 \times N$ convolutions, which are run stacks of the joint heatmap images.

Simple yet efficient real-time pose-based action recognition [38] was largely the inspiration for work done on this thesis. The goal of this paper was to provide a very lightweight and simple to understand intermediate representation that could be used by a very simple CNN to perform real-time action recognition. They do this by converting the skeletons into their unique Encoded Human Pose Image (EHPI), which is a 2 dimensional grid where the x-axis is frame index, and the y axis is the joint index, this is shown in figure 2.24. This EHPI representation can then be used with a very simple CNN to provide very fast and good results in order to process actions in real time. There is one notable disadvantage in that it relies so heavily on the

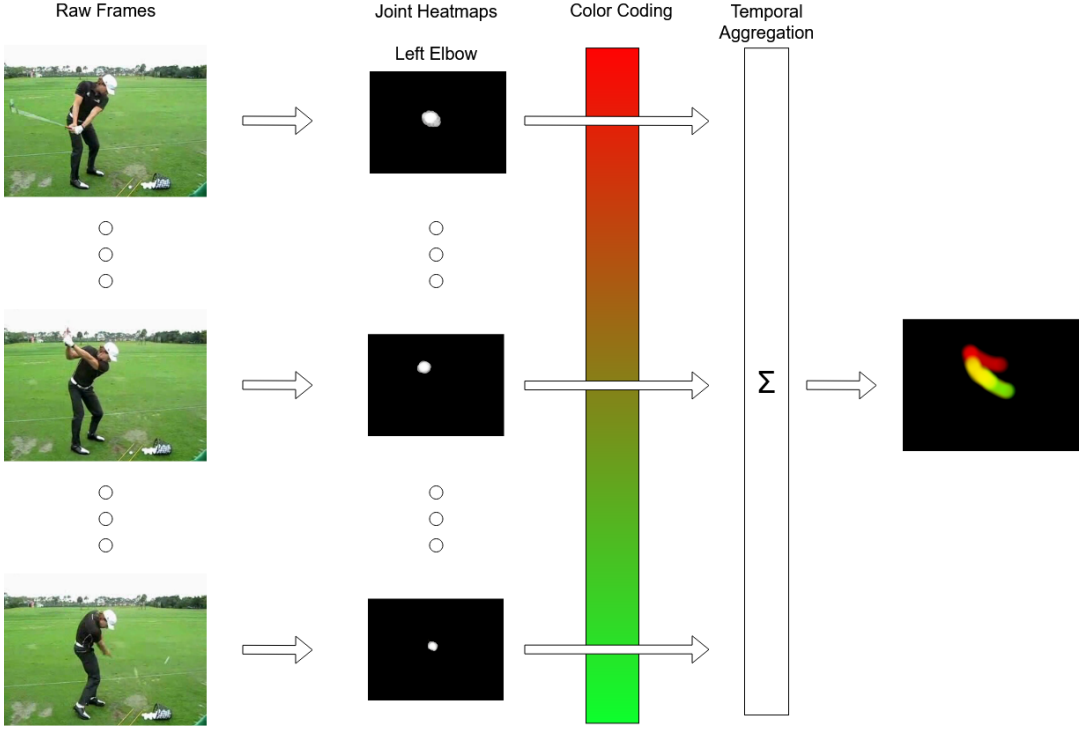


FIGURE 2.22: The illustration of the PoTion intermediate representation [35]. The input joint heatmaps are colored based on their time in the frame, and the frames are then concatenated to form the final movement of the joint throughout the video (the figure shows only one joint heatmap, the same process is followed for all other detected joints).

global positioning of the person in the frame. This means that the representation is very sensitive to things such as camera movement, where a slight movement results in the representation interpreting as the whole person sliding throughout the frame, however this could be mitigated via person detection to keep the person centered in the frame, however this introduces another point of failure.

Make Skeleton-based Action Recognition Model Smaller, Faster and Better [39] is yet another improvement on this intermediate representations, but with the particular focus on making the representations more resistant to both rotation & shifting of a person throughout the frame. As shown in figure 2.25, this is done through two features, the cartesian coordinate feature which was used in previous models in a similar way [38], and the Joint Collection Distances (JCD) feature. The JCD feature is indifferent to shifting since all of the representation is aware of is the distance between any two given joints. This allows for easier generalization, however in the final model, both the cartesian coordinate and JCD features are used,



FIGURE 2.23: The main PA3D [37] model architecture, demonstrating the 1x1 convolutions used in order to construct the temporal cube, in this case on the right wrist.

as the authors determined that both were key in achieving high performance.

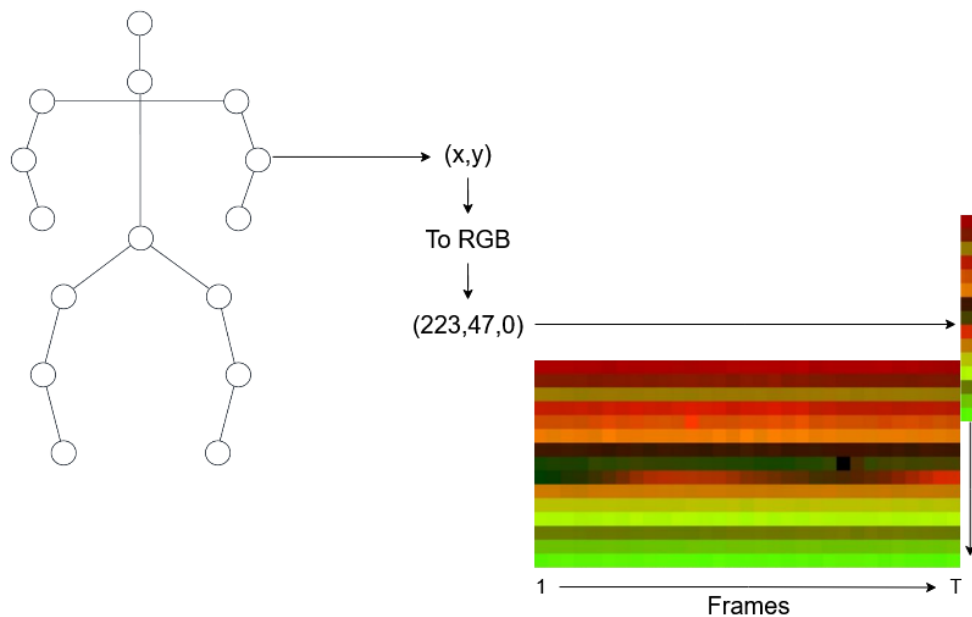


FIGURE 2.24: The EHPI representation used in the **Simple yet efficient real-time pose-based action recognition** [38]. The x , y coordinates of each joint are mapped to the red & green values of a pixel, all joints are then stacked to form a column of joint positions in a frame. Each frame is then placed next to each other to form the 2D representation. In the case of this representation the 'B' value of RGB is always 0 since we only have x and y values.

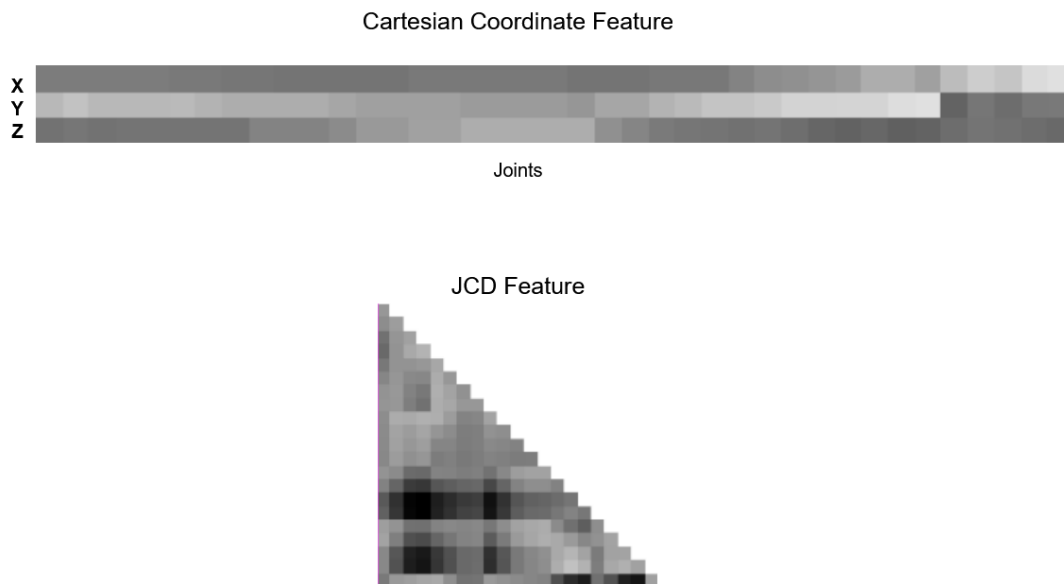


FIGURE 2.25: The representation used by the Smaller, Faster, Better model [39], this is split into two representations. The cartesian coordinates of each joint are encoded into a 2 dimensional representation, not dissimilar to previously discussed models [38]. The JCD feature is a similar representation, but instead of x , y , and z coordinates, uses the distance between two joints.

Chapter 3

Methodology

3.1 Dataset Selection

As has been stated previously in this thesis, the dataset that is used in the analysis of this model is JHMDB [28]. This dataset was selected for one primary reason, consistency when comparing one model to another. As was discussed in section 2.8, typical pose-based action recognition models utilize a two-step approach which involves first extracting pose data, then using that pose data in order to build intermediate representations. Usage of this dataset standardizes this first step since the pose data is included, rather than needing to be generated by a separate model. This means that a more direct comparison can be drawn from other models since the input data is all the same. It is an understood fact throughout the remainder of this thesis that small gains may be able to be made through the addition of a more accurate pose model, however the scope of this thesis specifically focuses on the intermediate representation and corresponding models that process this representation.

3.2 Pose

The methodology throughout this section is dependent on pose information output from models that were described in section 2.8. These pose models have several outputs used by similar models such as joint heatmaps, however the main focus of this paper is the positions of the joints. These joints can be connected by lines to form "bones" which are then all connected together to form a "skeleton". This skeleton is

shown in figure 3.1, where each of the joints are connected to form a human-like figure that can easily be created from the x & y coordinates of the joints.

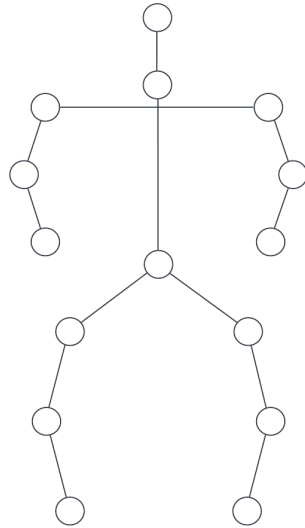


FIGURE 3.1: Example of how joints are connected through bones in a typical pose representations.

Using the JHMDB dataset, we simply take the existing pose implementation, the representation and indexes being shown in figure 2.16, with 15 total joints. Specifically in this thesis, we are concerned with bone-joint-bone connections, effectively representing the angle of the middle joint and how the bones around it move.

3.2.1 Joint Angles

The core of how the new representation will represent actions and movement has to do with the angle between two bones at any one given joint.

The first step in calculating the directional angle between the two vectors is to center one of the joints at the origin. Throughout this chapter, we will be referring to these two vectors as a and b . In figure 3.2, "a" would be denoting the vector $B \rightarrow A$ and "b" the vector $B \rightarrow C$. In this example, "B" will be the origin. This origin centering is simple and is done by the following equation 3.1, with each point representation as it was in figure 3.2 using the $B \rightarrow A$ bone as an example.

$$a(x, y) = (A.x - B.x, A.y - B.y) \quad (3.1)$$

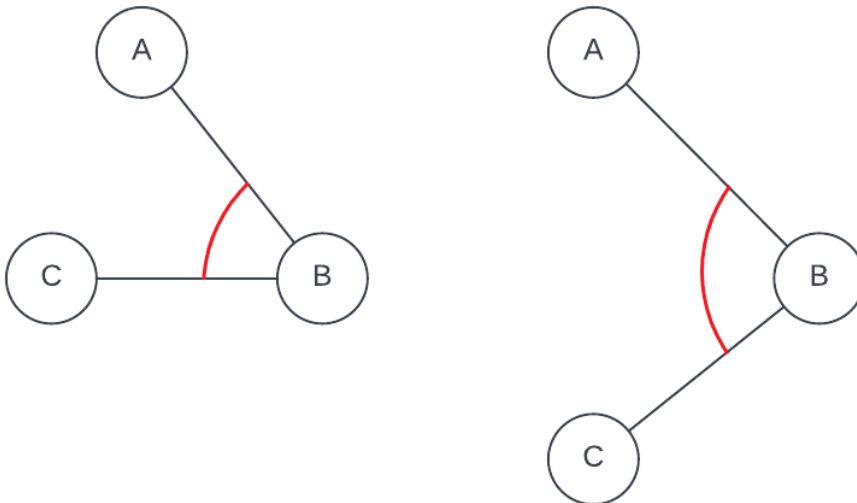


FIGURE 3.2: Two examples of three joints interconnected with two bones, and how the angle can change from one frame to another.

After processing both bones through this equation, it produces two vectors beginning at the origin. The goal then becomes calculating the angle between two of these vectors. This can be easily done by leveraging arctan. Calculating the angle of a given vector ' a ' to the x-axis is simply done by using $\arctan(a.y/a.x)$. Once we have the angle of this vector to the x-axis, we can convert it to a positive value to ensure that the angle is being measured from a clockwise direction. Afterwards, we simply take the difference of the two vectors to determine the clockwise directional angle between two given vectors as denoted in equation 3.2.

$$\arctan(a.y/a.x) - \arctan(b.y/b.x) \quad (3.2)$$

The angle is calculated in a particular direction because if it were simply to be calculated agnostic of direction, it would be impossible to determine what angle a joint moves if it were to cross the 180° boundary. Table 3.1 demonstrates this issue, where a 180° rotation is observed from one right angle to another, but if non-directional angle is used, no change is represented. This prevents us from using a simpler solution such as the dot product to calculate these angles.

a(x,y)	b(x,y)	Directional	Non-Directional
(1, 0)	(0, 1)	90°	90°
(1, 0)	(0, -1)	270°	90°

TABLE 3.1: Example of how non-directional angle can result in incorrect rotation changes from one frame to another.

The resulting method means that some angles will be measured from the "outside" of the person and some will be measured from the "inside" as shown in figure 3.3. In practice, this does not have a large effect on the representation as the primary factor in this method is the change of an angle from one frame to another which is indifferent to how the angle is measured as long as the distance is consistent.

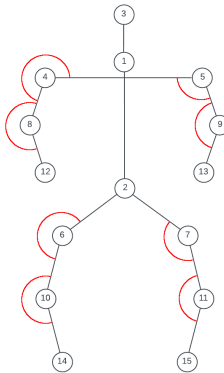


FIGURE 3.3: An example skeleton with JHMDB indices in each of the joints. In addition, angles have been shown as if they are being calculated in a clockwise direction, resulting in connections such as 5-4-8 having the angle on the "outside" of the person.

3.2.2 Joint Velocities

Once the joint angles for each frame have been extracted, the next step before implementation into our representation is to determine the change of a joint angle from one frame to another to determine the "velocity" of said joint angle. Generally this is simply done by calculating $\text{angle}(b) - \text{angle}(a)$, however there is one exception where the angle change crosses over the positive x-axis. This would be an example such as the difference between $\text{angle}_1 = 5$ and $\text{angle}_2 = 350$. The correct description would be that the angle moved -15° , however using that simple calculation would mean that the model would interpret this as a 345° change. This is most likely incorrect, as the more likely scenario is that the person moved -15° rather than almost a complete rotation in the other direction. So we add logic such that if the difference between two angles is greater than 180° or lower than -180° , the most likely scenario is that it moved in the opposite direction for a shorter distance. So a change such as 270° would become -90° and similarly a change of -270° would become 90° .

3.3 Novel Intermediate Representation

We can now construct the intermediate representation that will be used as input to our model. The model representation is very similar to that in the **Simple yet efficient real-time pose-based action recognition** [38] as described in section 2.9.1, which involves constructing a 2 dimensional image that is easily fed into a simple model. This is represented in figure 3.4, where one joint angle is taken from one frame of the video, and added to a column. This column consists of all of the data for one frame of the video, which is then added to the rest of the representation, eventually constructing the joint angles for each frame of the video.

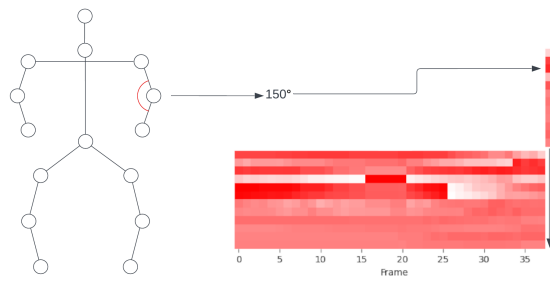


FIGURE 3.4: Example of how the intermediate representation is constructed. At each frame, the angles of each joint are taken and added to a column, each column is then stacked next to one another to form a 2 dimensional image.

As described previously in section 3.2.2, a key point of our representation is the joint velocities portion. These values can simply be "stacked" on top of the angles to form the full intermediate representation. The logic is that for any given frame i , the column contains both the joint angles for the frame i , as well as their differences between frame i and $i + 1$.

The specific joints that are represented in our intermediate representation are shown in table 3.2. These joints were chosen as they are major joints that form the typical "skeleton" visualization similar to that shown in figure 3.1 and 3.3.

3.3.1 Representation Features

The way the representation is constructed results in a representation that is 2-D rotation invariant, scale invariant, and global position invariant, providing us with advantages over other models.

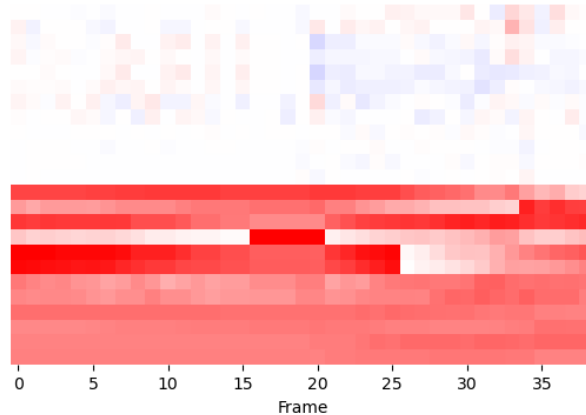


FIGURE 3.5: The finished intermediate representation, the top half contains the changes in joint angle from one frame to another (also referred to as "velocity"), and the bottom half contains the joint angles themselves. This is referred to as the "stacked" representation. In the representation, positive values are shown as red and negative values are shown as blue, with the higher values having more saturation.

Rotation does not affect the representation since the angle of a joint from one frame to another only relies on the two bones, the two bones can rotate globally, what matters is only the angle between the two given bones. This effect is shown in figure 3.6, where the angle of interest does not change when another joint next to it is rotated, this can be generalized to any global rotation with the same logic.

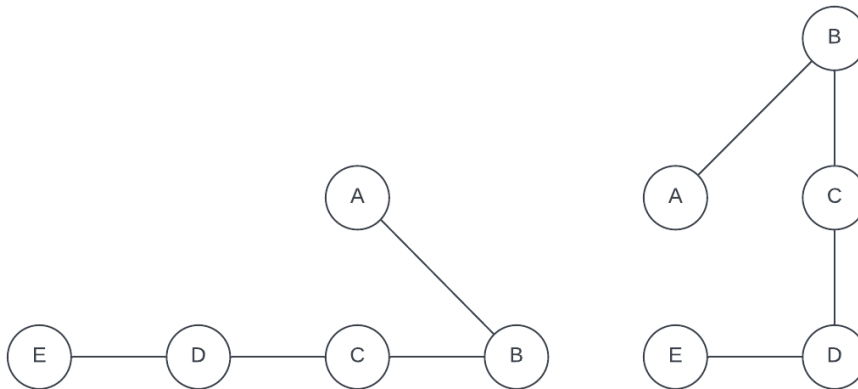


FIGURE 3.6: Example of the rotation invariance of our representation. The angle represented is $A - B - C$, and is unaffected by a rotation around $C - D - E$, remaining at 45° .

Scale is avoided entirely as we do not take into account the length of the bones, rather only the angle of the joints. As was stated previously in this chapter, the bones are converted to vectors prior to computing the angle between them. This involves normalizing both bones to be length one, and this length data is not held for any part of the representation. Therefore, the person can move closer or farther from the

Joint A	Joint B	Joint C	JHMDB Indices
Face	Neck	Right Shoulder	(3, 1, 4)
Face	Neck	Left Shoulder	(3, 1, 4)
Right Elbow	Right Shoulder	Left Shoulder	(8, 4, 5)
Left Elbow	Left Shoulder	Right Shoulder	(9, 5, 4)
Right Elbow	Right Shoulder	Right Hip	(8, 4, 6)
Left Elbow	Left Shoulder	Left Hip	(9, 5, 7)
Right Wrist	Right Elbow	Right Shoulder	(12, 8, 4)
Left Wrist	Left Elbow	Left Shoulder	(13, 9, 5)
Right Shoulder	Right Hip	Right Knee	(4, 6, 10)
Left Shoulder	Left Hip	Left Knee	(5, 7, 11)
Right Hip	Right Knee	Right Ankle	(6, 10, 14)
Left Hip	Left Knee	Left Ankle	(7, 11, 15)

TABLE 3.2: All Joint connections used in our intermediate representations. The joint angle that is focused on is centered on the **B** joint, with the two vectors $B \rightarrow A$ and $B \rightarrow C$ forming the angle used in the representation.

camera during the action, and it will have no effect on the representation.

Global Position is the final feature that the representation is invariant to. Similar to the previous features, the representation only cares about the angle of the specified joint, meaning that we can translate the person from one side of the frame to another with no change in the representation.

These three features of the model aim to mitigate background interference that has been previously discussed in the model. Specifically, they aim to reduce interference from movement of the camera. A person can move to either side, closer or farther away, and rotate the camera and there will be no effect on the representation.

3.3.2 Representation Comparison

Comparing our representation to other intermediate representations, there are many similarities that can be observed.

The overall structure of the representation was largely inspired by **Simple yet efficient real-time pose-based action recognition** [38], as shown in figure 3.7. While the construction of this 2 dimensional grid was a very efficient way to construct the representation, their representation relied on the cartesian coordinates, resulting in a representation more susceptible to background interference. However, the general structure of the image was adapted for our use, simply using a different data source (joint angles + velocities).

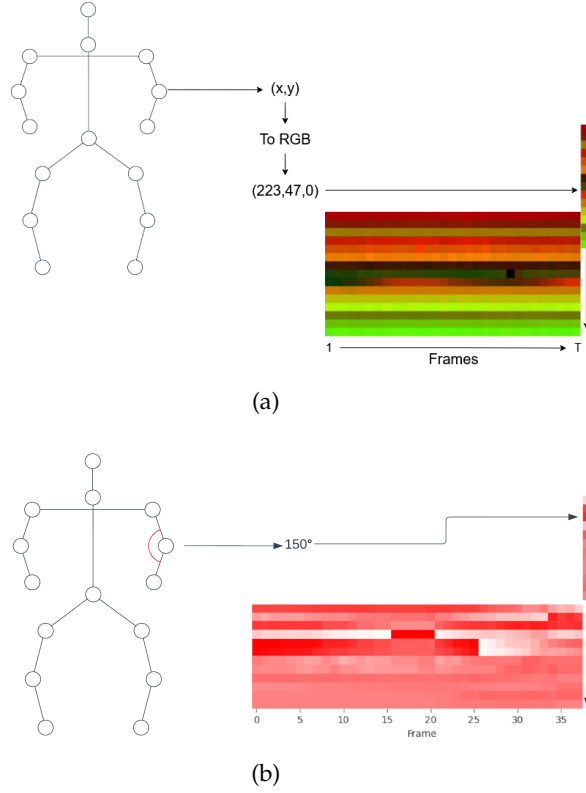


FIGURE 3.7: Comparison of our representation (b) compared to **Simple yet efficient real-time pose-based action recognition** [38] (a), showing a similar representation construction.

Make Skeleton-based Action Recognition Model Smaller, Faster and Better

[39] also contains a similar representation to ours. Their representation is broken into two parts: a cartesian coordinate feature and a JCD (Joint Collection Distances) feature. The cartesian coordinate feature is no different to that proposed in other representations [38], suffering from the same background interference. Their JCD feature is similar to ours in that it is only using the pose data, and resistant to background interference. Our representation differs in that rather than using both global and pose data, we restrict to only the pose data to completely eliminate background interference.

3.3.3 Temporal Adjustments

It is not unreasonable to assume that moving from only one frame to the next would result in some actions not being represented as well as other actions (this is shown in figure 3.8). Due to this issue, we add a temporal adjustment to our representation in

order to better represent some of these actions. This is done by adding more channels to the data, with each of the channels "skipping" frames. This would mean that rather than having the angle difference representation moving from frames $1 \rightarrow 2 \rightarrow 3$, in the first additional channel it would move from frames $1 \rightarrow 3 \rightarrow 5$. The representation is then padded out to fit the same shape and added as another channel to the data. This is more clearly shown in figure 3.9 where the actions become more "compressed" and movements over longer periods of time become easier to visualize and process.

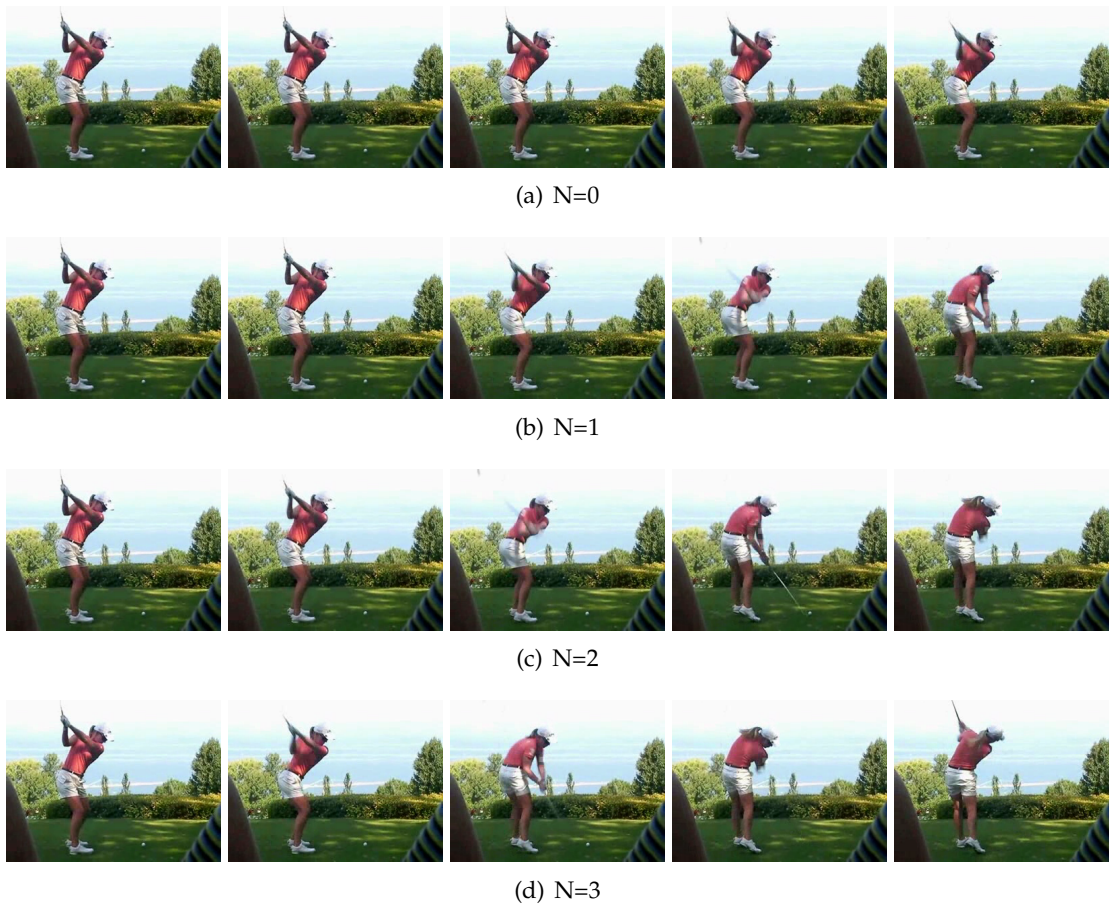


FIGURE 3.8: An example of the temporal adjustment on the golf action, skipping N frames between each image. As can be seen in (a), the movement is not as pronounced and the model may have difficulty determining the action because the velocity of the person is not very pronounced. When observing examples (c) and (d), the full action from one frame to another is much more clear and the deciphering of the intermediate representation would be easier as the movement is more pronounced.

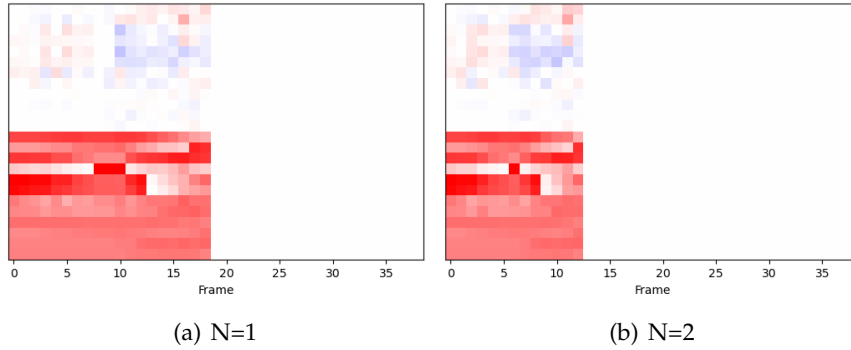


FIGURE 3.9: Two examples of temporal adjustment to the stacked representation. In both cases, the representation skips N frames in each step, meaning with a $N = 1$ the representation will ignore every other frame, $N = 2$ every two frames, etc. As can be seen from the joint velocities, with example (b), the joint velocities are more intense and concentrated.

3.3.4 Model Architecture

The goal of this intermediate representation is to be able to use a simple 2-dimensional CNN which is able to run on simpler and less expensive hardware. The simplified architecture diagram in figure 3.10 shows the simple CNN architecture that is to be used. The model consists of 3 convolutional layer groups, followed by global average pooling and the final classification layer. Each individual layer and a more detailed breakdown is shown in table 3.3.

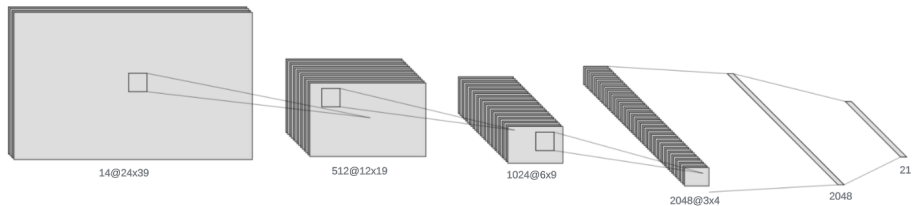


FIGURE 3.10: The basic model architecture used, very similar to that used in other models such as Potion [35], it is a simple 2 dimensional CNN that contains one fully connected layer at the end for classification.

This network is similar to the VGG-16 model previously discussed in section 2.3 and seen in figure 2.4, which is a proven image classification model. Because of the nature of the created intermediate representation, the task can be shifted from processing video to a more classical task of image classification.

Figure 3.11 shows the overview of the model from RGB frames to output. This diagram demonstrates the full pipeline and the overall simplicity of our approach.

2D Convolution @ 512 Channels 2D Batch Normalization ReLU 2D Convolution @ 512 Channels 2D Batch Normalization ReLU 2D Max Pooling
50% Dropout 2D Convolution @ 1024 Channels 2D Batch Normalization ReLU 2D Convolution @ 1024 Channels 2D Batch Normalization ReLU 2D Max Pooling
50% Dropout 2D Convolution @ 2048 Channels 2D Batch Normalization ReLU 2D Convolution @ 2048 Channels 2D Batch Normalization ReLU 2D Max Pooling
Global Average Pooling Flatten 21 Class Softmax Layer

TABLE 3.3: The detailed breakdown of the model architecture, split into 3 convolutional blocks and one dense layer used for classification. All convolutional layers utilize 3x3 convolutions, including a 1 pixel padding across all sides. The 2D max pooling utilized a 2x2 kernel, halving the size of the images after each convolutional block.

As has been stated previously in this thesis, the pose estimation model is not fully explored in combination with our model, however when considering an in-the-wild approach it is an important part of the pipeline. This could be similar to the previously discussed OpenPose [30] model as discussed in section 2.8, or a much lighter model that can be run on less modern or mobile hardware.

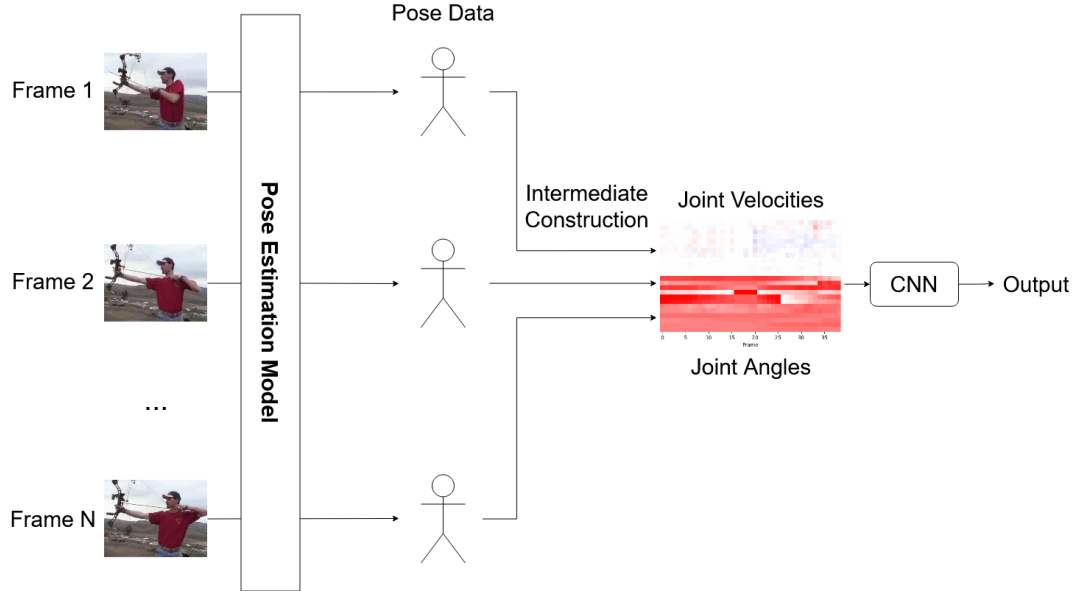


FIGURE 3.11: Block diagram showing our intermediate representation from start to finish, including the pose estimation model that was not explored in this thesis.

This model architecture is very similar to that used in similar papers that construct these intermediate representations. These models have near identical structures to both each other and our proposed end model, with several convolutional layers, followed by a global average pooling, and finally dense layers. As has been stated before, this structure is a classical image classification architecture similar to that of VGG-16 [11], which is a proven effective model in the image classification task. Our model differs slightly in that it contains many more filters than the similar models. While we explored models similar to that used in similar approaches, it was found that using significantly more filters in the convolutions lead to a very large increase in performance, so lower amounts of filters were abandoned in favour of the more complex model.

The model was trained using the stochastic gradient descent (SGD) optimizer, with an initial learning rate of 0.01, momentum of 0.9, batch size 16, and weight decay 0.005. After each epoch, the learning rate was multiplied by 0.999, reducing the learning rate gradually over the training period. As the dataset was well balanced with the training and testing datasets and the classes had an even number of examples, the only augmentation was a shuffle operation before each epoch.

Chapter 4

Experimentation

4.1 Compute Resources

The model was mainly trained on a single **NVIDIA GeForce 3090** GPU, which as of writing is one of the highest end graphics cards. However, this GPU is significantly more compute power than is needed in order to train the model. The GPU used to train this model has 24 GB memory, whereas the model typically only utilizes 3.5 GB GPU memory maximum at train time. This would in theory mean the model could be trained on less modern, cheaper hardware such as the **NVIDIA GeForce GTX-1660**. The model is also almost certainly compact enough to be trained without GPU acceleration, however this would result in large training time increases, so for the purposes of this thesis it was not explored.

4.2 JHMDB Results

The dataset that the model will be evaluated on will be the JHMDB dataset. As previously stated in section 2.7, JHMDB is a good dataset to evaluate performance on pose-based models. The dataset contains 3 splits, each of which have a training and testing pair. Three independent models will be trained, one on each of the splits, without any previous pre-training, and with randomly initialized weights that will be seeded such that they're consistent from one run to another.

Table 4.1 contains the accuracy results of the previously discussed model and representation on the JHMDB dataset. As can be seen the model obtains on average a 58% testing accuracy using only the novel approach presented. This accuracy alone

Split	Accuracy
1	58.209%
2	58.889%
3	58.113%
Average	58.404%

TABLE 4.1: Results on all 3 splits of the JHMDB dataset utilizing only our novel approach.

is not quite sufficient to show that the model is capable of action recognition, however as will be shown further in this chapter, the model is much more capable when predicting some actions, showing some potential with this compact representation.

$$F1 = 2 \cdot \frac{precision \cdot recall}{precision + recall} \quad (4.1)$$

These accurate results do not tell the complete story however. As can be seen from the individual class F1 scores in figure 4.1 (the equation for calculating F1 score is shown in equation 4.1, where precision is the percentage of predicted examples that are correct, and recall is the percentage of examples for any given class that are correctly predicted), the model is fairly good at predicting classes that have very clear movements associated with them such as *golf*, *pullup*, or *swing_baseball*. The significance of these classes is that the variance of the movement from one person to another is not very significant, so the model is able to learn the joint movements and apply that logic to other examples. Meaning the model is very good at recognizing these actions in any given environment.

The opposite factor is also something to consider. Figure 4.2 shows an example of three different sets of frames from the *jump* class, which had an average F1 score of approximately 0.3. As can be seen from the frames, there are many different ways that a person may perform the *jump* action. A good example is the final two frames from figure 4.2(a), where the person simply moves throughout the global position of the frame, rather than actually moving any of their joints. Comparing to figures 4.2(b) or 4.2(c), where there are many joint movements throughout the frames, makes it difficult for the model to interpret them as the same and generalize to other examples of the same class. Figures 4.2(b) and 4.2(c) also demonstrate the variability in how these actions can be performed, where 4.2(b) shows more of a twisting motion,

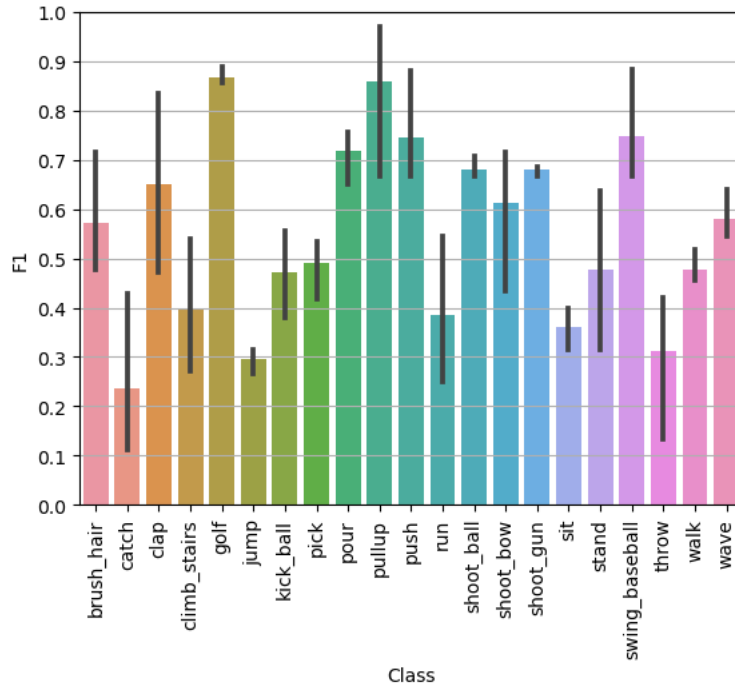


FIGURE 4.1: Detailed F1 score results on the JHMDB dataset, averaged over the 3 testing splits. Black bars show the corresponding maximum & minimum values attained in one of the splits.

4.2(c) is a more typical "straight on" jump.

This low variability in the *golf* class can also be demonstrated in a similar fashion to this. Figure 4.3 demonstrates this behaviour, where the action is nearly always performed in the same way where a person is standing, reaches back, twists and pulls the club forwards. Figures 4.3(a) and 4.3(c) are perhaps the best examples as they are swinging similar clubs, so the way that they move is almost identical, therefore meaning that the intermediate representation will also be similar. Figure 4.3(b) is again a very similar movement, however it is a slightly different club meaning the movement is not as pronounced.

The detailed precision and recall values broken down by class are shown in figures 4.4 and 4.5, and in general reflect the same results as the F1 scores. The only notable difference is the model tends to have more volatile recall whereas precision tends to be closer from one class to another. This can be seen more clearly in classes such as *golf*, *pour*, *pullup*, and *push* which have a very high recall compared to some other classes, but the precision is closer when compared to the other classes.

We can further explore the results as shown in figure 4.6. These matrices for each split demonstrate that overall, the model predicts the correct class quite well.

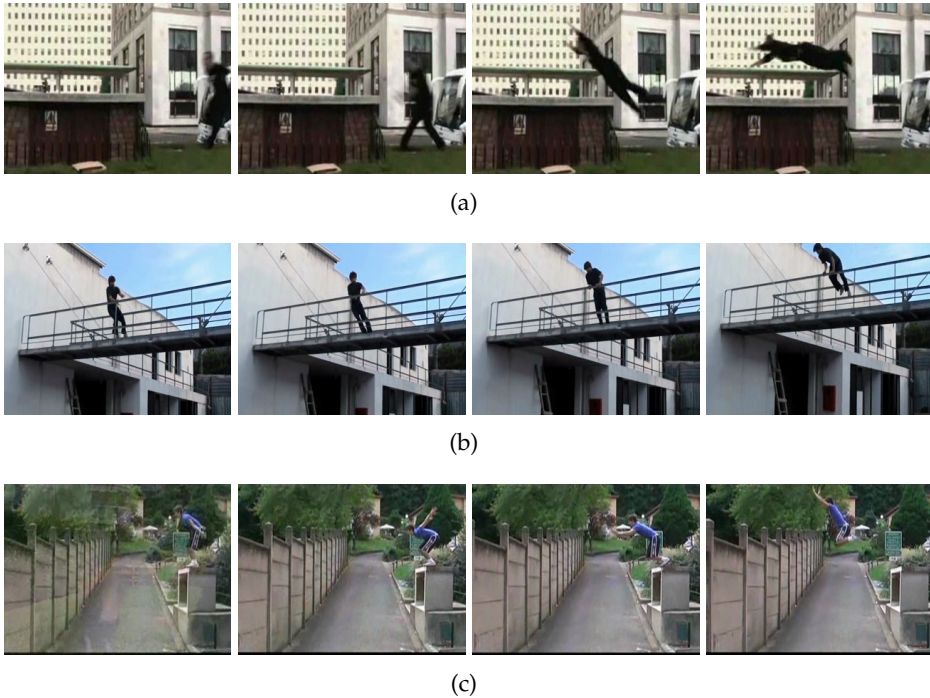


FIGURE 4.2: Three examples of the *Jump* class from the JHMDB dataset. The frames selected were four frames roughly evenly spaced out through the video.

However it does tend to get confused in particular cases when the actions are similar, this will be further explained in when we study the failure cases in the next section.

4.3 Failure Cases

There are some specific failure cases that are worth observing, similar to the example shown in figure 4.2. These failure cases are important to understanding how the model uses the representation and further examining the types of actions that the model has difficulty with outside of the previously discussed high variability in some actions.

Figure 4.7 shows an example of the catch action. The primary issue is that throughout the four frames, there is very little movement by the main person who is performing the action of catching the ball. Due to the fact that the representation relies heavily on movement from one frame to another, this means that about 50% of the representation is not used effectively because there is not very much movement. The underlying issue is that the model cannot see any person-object interactions. Other models that process the RGB frames or optical flow are able to pick up on



FIGURE 4.3: Three examples of the *Golf* class from the JHMDB dataset. The frames selected were four frames roughly evenly spaced out through the video.

the ball moving from one person to another, whereas our model cannot detect this object.

Another problem class is the sit action shown in figure 4.8. Our representation is designed in a way such that global position is not considered, which is an intentional decision in order to add some more ability for the model to generalize. This however also has some other consequences, as can be seen by the given example. The person does not have very much movement in their upper body, only pivoting at the hip. The crucial note that they are performing a "sit" rather than another action is their movement down through the frame. This global position change is not detectable by our representation and results in the model performing poorly for this class.

While the variability of actions is generally considered good for accuracy, this can also be detrimental to the performance of the model if two actions have very similar movements. This is shown in figure 4.9, where the actions shown (walk and climb stairs) have very similar movements. They differ only in two aspects. First, the climb stairs action generally moves the person vertically through the frame throughout. Second is that there are context clues in the background such as a lack of staircase in the run action, whereas the climb stairs action always has a staircase. In both

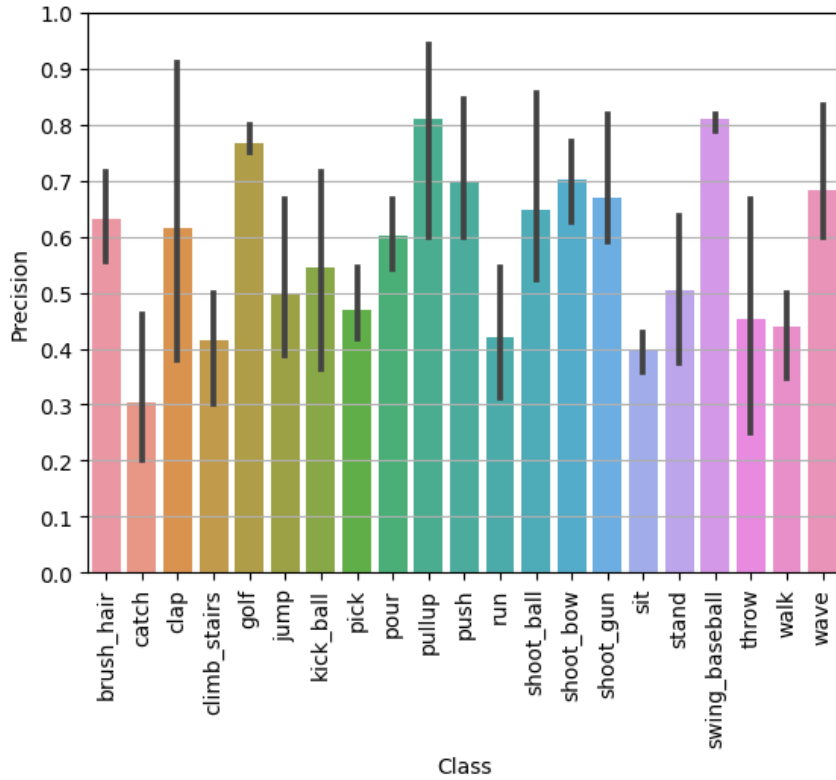


FIGURE 4.4: Detailed precision results on the JHMDB dataset, averaged over the 3 testing splits. Black bars show the corresponding maximum & minimum values attained in one of the splits.

of these cases, our model is not able to take this information in, resulting in the run and climb stairs actions looking similar in our representation, and making it difficult to distinguish between the two, resulting in the poor performance for both classes. As stated previously, this effect can be seen more in detail in figure 4.6, where it is shown that the model quite often confuses climb stairs and walk.

4.4 Model Ablation Study

This section will present both different intermediate representation formats, as well as different model architectures. The natural first step to determining how effective the chosen architecture compared to others is to isolate each of the two halves (angle velocities & angles themselves). These results are presented in tables 4.2 and 4.3.

The only angle velocity results show an average decrease in performance over all three splits of approximately 14% over the combination of the two. This is a very large decrease in accuracy, but is far from a negative result. What this result shows

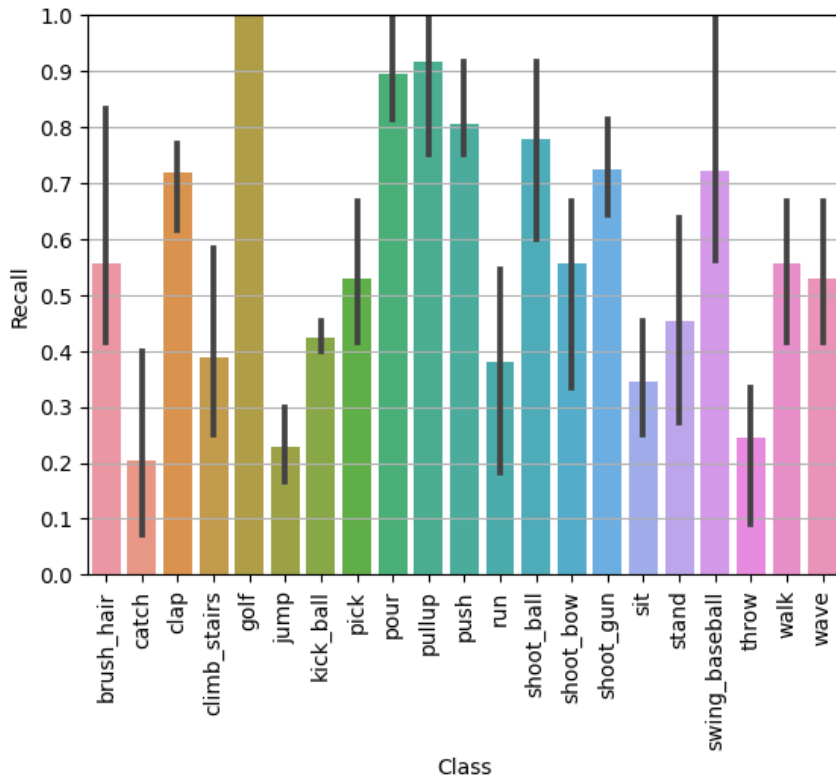


FIGURE 4.5: Detailed recall results on the JHMDB dataset, averaged over the 3 testing splits. Black bars show the corresponding maximum & minimum values attained in one of the splits.

Split	Stacked	Only Angle Velocity
1	58.209%	48.888%
2	58.889%	44.444%
3	58.113%	41.132%
Average	58.404%	44.821%

TABLE 4.2: Comparison of results using only angle velocities vs the stacked representation.

is that for some classes, the actual movement of the joint can be used in place of the joint angles and it is not necessarily required to have both in the representation. This is shown in figure 4.10, where we see that classes such as golf & pullup still have a relatively high F1-Score of 0.7 on average.

Similarly, the representation that uses only angles and ignores the angle velocities shows a decrease in performance, as seen in table 4.3. This is much less pronounced, and is only around 1%. This suggests that while the angle velocities do add value, it is not uniformly a large positive. However when considering how small the added data is in the stacked representation the small increase in accuracy

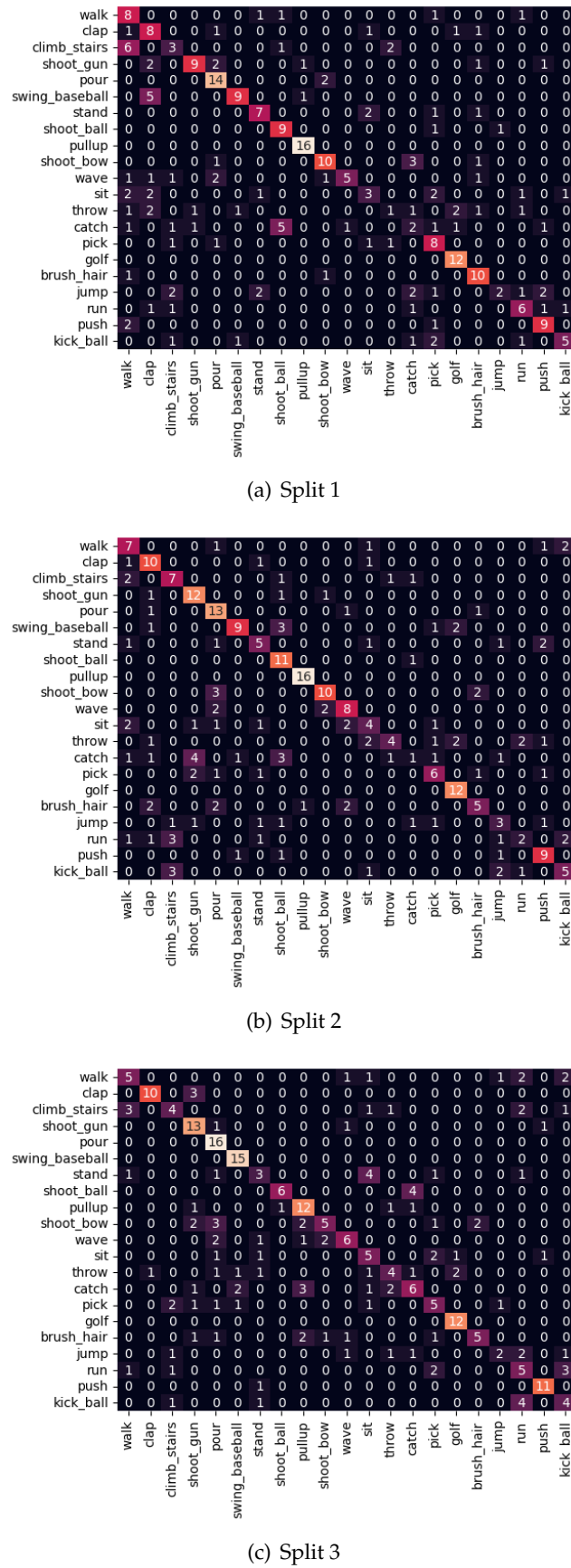


FIGURE 4.6: Confusion matrices for each of the 3 JHMDB splits.



FIGURE 4.7: An example of the **catch** action from the JHMDB dataset [28].



FIGURE 4.8: An example of the **sit** action from the JHMDB dataset [28].

is justified.

Another intermediate representation was also explored as is shown in figure 4.11, where rather than "stacking" the angles and velocities on top of one another, we "interlace" the joint angles and their corresponding velocities. The idea behind this representation being that the initial CNN filters would overlap between each individual joint angle and their corresponding velocity, meaning that the model may be able to learn these relationships a bit better.

The results of this interlaced representation are shown in table 4.4. The results show on average a 4% decrease in performance when compared to the stacked model. This is almost certainly because the model benefits more from the convolutions being run on the angles and velocities independently and combining later in the model after pooling layers rather than on both the angles and velocities initially.

With this knowledge that the model typically performs better with the different features being stacked on top of each other and somewhat isolated, the next step was to see if further isolating the angles and velocities from one another would result in more performance gain. This resultant architecture is shown in figure 4.12, where we split the angles and velocities completely, mimicking the fusion-based architectures as were shown previously in figure 2.20, where these models tended to split RGB, Optical Flow & Pose data we similarly split our two pose joint features.

As can be seen from the results in table 4.5, once again this change to the model

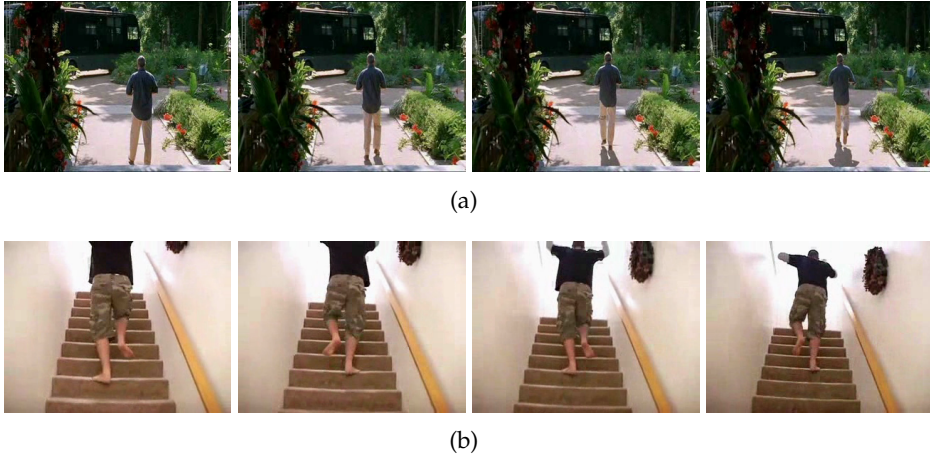


FIGURE 4.9: Comparison between the **walk** (a) and **climb stairs** (b) actions from the JHMDB dataset [28] showing similar movements.

Split	Stacked	Only Angles
1	58.209%	56.343%
2	58.889%	58.889%
3	58.113%	56.604%
Average	58.404%	57.279%

TABLE 4.3: Comparison of results using only angles vs the stacked representation.

results in a decrease in performance by approximately 10%. This reduction in performance is most likely because of the increase in complexity to the model, it overfit the relatively small dataset much more easily, meaning that it was less easily able to generalize. It may also be due to the fact that in the stacked representation, the combination of angles and velocities can be "learned" as the convolutions combine them at each step, whereas the split model isolates them until the very end, potentially losing data in the process.

We can also examine utilizing deeper and shallower networks with this representation. A shallower model would allow us to further reduction in memory needed to both train the model as well as a reduction in the hardware required to run the model in production scenarios. A larger model could potentially allow for an increase in performance while sacrificing some of the advantages described previously. Table 4.6 shows these results, the results from both shallow & deep models are outperformed by our proposed model. An exception is split 3 of the shallow model which outperforms our proposed model, however the average between the three splits is significantly lower. This is most likely due to the smaller model having slightly more

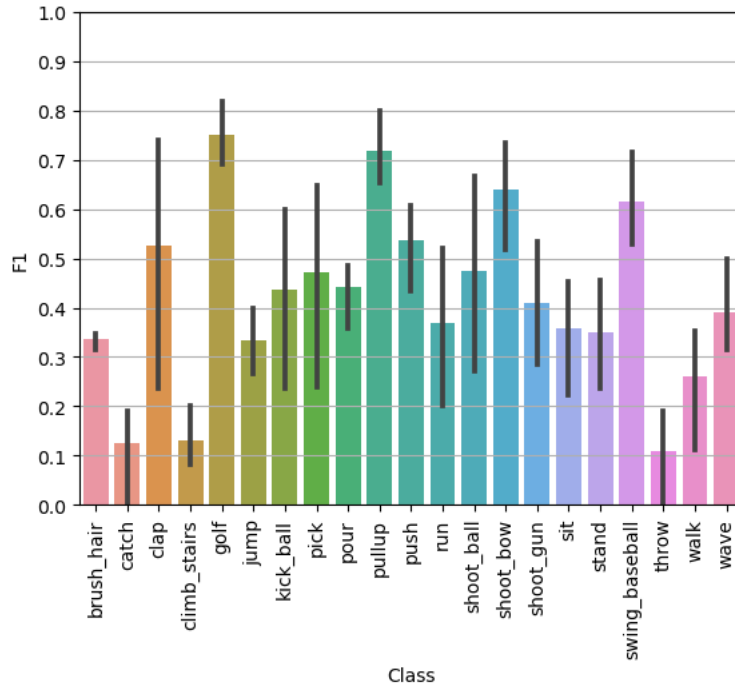


FIGURE 4.10: Detailed F1 score results on the JHMDB dataset using only the angle velocities from one frame to another.

Split	Stacked	Interlacing
1	58.209%	54.850%
2	58.889%	55.556%
3	58.113%	52.830%
Average	58.404%	54.412%

TABLE 4.4: Comparison of results using the interlacing vs stacked representation.

volatility when it comes to each of the splits and results therefore varying more than our proposed model from one split to another.

4.5 Model Comparison

When comparing our model and representation to others that are similar, it is important to note the difference in expected performance of our model vs. complex state of the art models. For this purposes of this thesis, we compare our model to other pose-based models, not taking into account those complex models that take very large GPU's to train, as this would be an unfair comparison.

As can be seen from the results in table 4.7, our model is not aiming to be the current state-of-the-art in it's category, however the performance is similar to the other

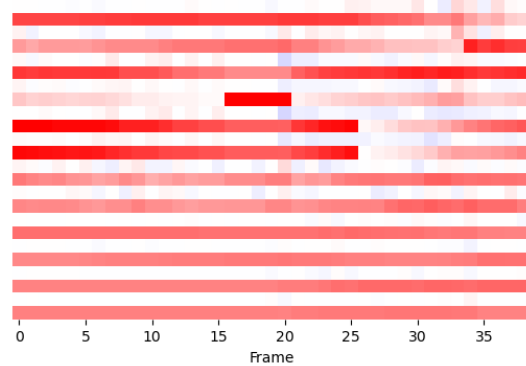


FIGURE 4.11: Alternative intermediate representation format where angles and velocities are interlaced rather than stacked.

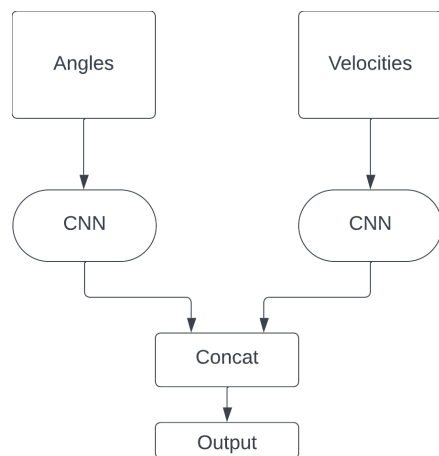


FIGURE 4.12: The split model architecture inspired by fusion models where the two different pose features are split and utilize independent CNN's.

models that approach the problem in a similar pose-based way. It is also notable, that our model is one of the only models that is both global position-invariant and scale-invariant, which is a large advantage of our model, and is by design as stated previously in this thesis.

	Split	Stacked	Split Representation
1	58.209%	46.269%	
2	58.889%	48.889%	
3	58.113%	49.811%	
Average	58.404%	48.323%	

TABLE 4.5: Comparison of results using the split model and representation against the single CNN stacked representation.

	Split	Standard Model	Shallow Model	Deep Model
1		58.209%	55.597%	55.970%
2		58.889%	57.407%	58.519%
3		58.113%	59.245%	53.585%
Average		58.404%	57.416%	56.025%

TABLE 4.6: Comparison of results using the final model compared to a shallower model using one less convolutional layer group, as well as a deeper model containing one additional convolutional layer group.

Model	Average JHMDB Accuracy
Chained [34]	56.8%
Potion [35]	57.0%
DynaMotion [40]	60.2%
EHPI [38]	60.5%
P-CNN [33]	61.1%
SIP-Net [41]	62.4%
STAR-Net [42]	64.3%
Pose & Joint Aware [36]	68.55%
PA3D* [37]	69.5%
Smaller, Faster, Better [39]	77.2%
Ours	58.404%

TABLE 4.7: Model comparisons that do not contain very complex models and utilize mainly pose data. * - PA3D uses additional data in its representation as well.

Chapter 5

Conclusion & Future Work

In this thesis, we have provided a novel representation for use in action recognition. This novel representation is unique to many other models in that it is invariant to:

- Scale
- Global Position
- 2-D Rotation

We explore many different variations of this representation, concluding that the best representation contains both joint angle data and joint angle velocity data, however, only angle data also provides good results. It was also found that this data functions the best as a single image, with one data source stacked on top of another. This means that the combining of the angles and velocities can be learned by the convolutions slowly over the entire model, rather than typical fusion-like architectures that concatenate the different sources at the end.

With this representation, we were able to leverage a simple CNN model that is trainable on lightweight GPU's and is able to be tested on even lighter hardware. Despite the model being relatively lightweight, the model is able to provide 58.404% average accuracy over the 3 splits of the JHMDB dataset. This shows that despite the model not having been fed any data about how the person is moving globally, any data regarding the objects the person is interacting with, or any data about the environment it is able to fairly accurately predict what action the person is performing.

After further analyzing the results, the accuracy was shown to be slightly more nuanced than simply 58% accurate overall. The model was able to predict classes

that had more consistent movements that varied less from person to person such as golf or pullups, and tended to struggle with movements that can vary from person to person much more such as jump or catch.

5.0.1 Future Work

There is significant room for future work in this specific domain. Utilizing the skeleton data of a person to assist with action recognition is constantly evolving, and has continually been proved to help existing models improve on their results. However, a perhaps more interesting area of research that is not quite as popular is intermediate representations, which is where the "low hanging fruit" are. The first place of improvement would be to make the representation truly rotationally invariant, this would have to be done through 3-dimensional pose detection, and modifications of how changes in rotations are represented in the end image.

Another path forward is to more fully examine how real-time pose detection algorithms can be integrated with this simple model in order to obtain very fast and real-time results. This real-time computation is becoming more and more relevant in the world of smartphones, and examining how the model is able to be used on smartphones is crucial to determine the industrial applications. It is also worth noting that implementing this representation into existing complex models may be of interest in some applications, however the appeal of the representation being very lightweight and mobile applications not being as relevant cannot be ignored.

Bibliography

- [1] H. Sun and Y. Chen, *Real-time elderly monitoring for senior safety by lightweight human action recognition*, 2022. arXiv: [2207.10519 \[cs.CV\]](#).
- [2] A. Krizhevsky, G. Hinton, *et al.*, “Learning multiple layers of features from tiny images,” 2009.
- [3] M. Tan and Q. V. Le, *Efficientnetv2: Smaller models and faster training*, 2021. arXiv: [2104.00298 \[cs.CV\]](#).
- [4] P. Foret, A. Kleiner, H. Mobahi, and B. Neyshabur, *Sharpness-aware minimization for efficiently improving generalization*, 2021. arXiv: [2010.01412 \[cs.LG\]](#).
- [5] T. Ridnik, G. Sharir, A. Ben-Cohen, E. Ben-Baruch, and A. Noy, *Ml-decoder: Scalable and versatile classification head*, 2021. arXiv: [2111.12933 \[cs.CV\]](#).
- [6] J. Carreira and A. Zisserman, “Quo vadis, action recognition? a new model and the kinetics dataset,” in *proceedings of the IEEE Conference on Computer Vision and Pattern Recognition*, 2017, pp. 6299–6308.
- [7] C. Zach, T. Pock, and H. Bischof, “A duality based approach for realtime tv-l1 optical flow,” in *Pattern Recognition*, F. A. Hamprecht, C. Schnörr, and B. Jähne, Eds., Berlin, Heidelberg: Springer Berlin Heidelberg, 2007, pp. 214–223, ISBN: 978-3-540-74936-3.
- [8] Y. LeCun, Y. Bengio, and G. Hinton, “Deep learning,” *nature*, vol. 521, no. 7553, pp. 436–444, 2015.
- [9] Y. LeCun, L. Bottou, Y. Bengio, and P. Haffner, “Gradient-based learning applied to document recognition,” *Proceedings of the IEEE*, vol. 86, no. 11, pp. 2278–2324, 1998.

- [10] A. Krizhevsky, I. Sutskever, and G. E. Hinton, "Imagenet classification with deep convolutional neural networks," in *Advances in Neural Information Processing Systems*, F. Pereira, C. Burges, L. Bottou, and K. Weinberger, Eds., vol. 25, Curran Associates, Inc., 2012. [Online]. Available: https://proceedings.neurips.cc/paper_files/paper/2012/file/c399862d3b9d6b76c8436e924a68c45b-Paper.pdf.
- [11] K. Simonyan and A. Zisserman, "Very deep convolutional networks for large-scale image recognition," *arXiv preprint arXiv:1409.1556*, 2014.
- [12] K. He, X. Zhang, S. Ren, and J. Sun, *Deep residual learning for image recognition*, 2015. arXiv: [1512.03385 \[cs.CV\]](https://arxiv.org/abs/1512.03385).
- [13] F. Wang, M. Jiang, C. Qian, et al., *Residual attention network for image classification*, 2017. arXiv: [1704.06904 \[cs.CV\]](https://arxiv.org/abs/1704.06904).
- [14] J. Donahue, L. A. Hendricks, M. Rohrbach, et al., "Long-term recurrent convolutional networks for visual recognition and description," *IEEE Transactions on Pattern Analysis and Machine Intelligence*, vol. 39, no. 4, pp. 677–691, 2017. DOI: [10.1109/TPAMI.2016.2599174](https://doi.org/10.1109/TPAMI.2016.2599174).
- [15] W. Zaremba and I. Sutskever, *Learning to execute*, 2015. arXiv: [1410.4615 \[cs.NE\]](https://arxiv.org/abs/1410.4615).
- [16] Z. Qin, F. Yu, C. Liu, and X. Chen, "How convolutional neural networks see the world — a survey of convolutional neural network visualization methods," *Mathematical Foundations of Computing*, vol. 1, pp. 149–180, Jan. 2018. DOI: [10.3934/mfc.2018008](https://doi.org/10.3934/mfc.2018008).
- [17] M. D. Zeiler and R. Fergus, *Visualizing and understanding convolutional networks*, 2013. arXiv: [1311.2901 \[cs.CV\]](https://arxiv.org/abs/1311.2901).
- [18] J. Y.-H. Ng, M. Hausknecht, S. Vijayanarasimhan, O. Vinyals, R. Monga, and G. Toderici, "Beyond short snippets: Deep networks for video classification," in *2015 IEEE Conference on Computer Vision and Pattern Recognition (CVPR)*, 2015, pp. 4694–4702. DOI: [10.1109/CVPR.2015.7299101](https://doi.org/10.1109/CVPR.2015.7299101).
- [19] C. Szegedy, W. Liu, Y. Jia, et al., "Going deeper with convolutions," in *Proceedings of the IEEE Conference on Computer Vision and Pattern Recognition (CVPR)*, 2015.

- [20] S. Ji, W. Xu, M. Yang, and K. Yu, "3d convolutional neural networks for human action recognition," *IEEE Transactions on Pattern Analysis and Machine Intelligence*, vol. 35, no. 1, pp. 221–231, 2013. DOI: [10.1109/TPAMI.2012.59](https://doi.org/10.1109/TPAMI.2012.59).
- [21] D. Tran, L. Bourdev, R. Fergus, L. Torresani, and M. Paluri, *Learning spatiotemporal features with 3d convolutional networks*, 2015. arXiv: [1412.0767 \[cs.CV\]](https://arxiv.org/abs/1412.0767).
- [22] A. Dosovitskiy, L. Beyer, A. Kolesnikov, et al., *An image is worth 16x16 words: Transformers for image recognition at scale*, 2021. arXiv: [2010.11929 \[cs.CV\]](https://arxiv.org/abs/2010.11929).
- [23] S. Yan, X. Xiong, A. Arnab, et al., "Multiview transformers for video recognition," in *Proceedings of the IEEE/CVF Conference on Computer Vision and Pattern Recognition (CVPR)*, 2022, pp. 3333–3343.
- [24] G. A. Sigurdsson, G. Varol, X. Wang, A. Farhadi, I. Laptev, and A. Gupta, *Hollywood in homes: Crowdsourcing data collection for activity understanding*, 2016. arXiv: [1604.01753 \[cs.CV\]](https://arxiv.org/abs/1604.01753).
- [25] A. Gorban, H. Idrees, Y.-G. Jiang, et al., *THUMOS challenge: Action recognition with a large number of classes*, <http://www.thumos.info/>, 2015.
- [26] W. Kay, J. Carreira, K. Simonyan, et al., *The kinetics human action video dataset*, 2017. arXiv: [1705.06950 \[cs.CV\]](https://arxiv.org/abs/1705.06950).
- [27] K. Soomro, A. R. Zamir, and M. Shah, *Ucf101: A dataset of 101 human actions classes from videos in the wild*, 2012. arXiv: [1212.0402 \[cs.CV\]](https://arxiv.org/abs/1212.0402).
- [28] H. Jhuang, J. Gall, S. Zuffi, C. Schmid, and M. J. Black, "Towards understanding action recognition," in *International Conf. on Computer Vision (ICCV)*, Dec. 2013, pp. 3192–3199.
- [29] H. Kuehne, H. Jhuang, E. Garrote, T. Poggio, and T. Serre, "Hmdb: A large video database for human motion recognition," in *2011 International conference on computer vision*, IEEE, 2011, pp. 2556–2563.
- [30] Z. Cao, T. Simon, S.-E. Wei, and Y. Sheikh, "Realtime multi-person 2d pose estimation using part affinity fields," in *Proceedings of the IEEE conference on computer vision and pattern recognition*, 2017, pp. 7291–7299.
- [31] Y. Xu, J. Zhang, Q. Zhang, and D. Tao, *Vitpose: Simple vision transformer baselines for human pose estimation*, 2022. arXiv: [2204.12484 \[cs.CV\]](https://arxiv.org/abs/2204.12484).

- [32] M. Abadi, A. Agarwal, P. Barham, *et al.*, *TensorFlow: Large-scale machine learning on heterogeneous systems*, Software available from tensorflow.org, 2015. [Online]. Available: <https://www.tensorflow.org/>.
- [33] G. Chéron, I. Laptev, and C. Schmid, “P-cnn: Pose-based cnn features for action recognition,” in *2015 IEEE International Conference on Computer Vision (ICCV)*, 2015, pp. 3218–3226. DOI: [10.1109/ICCV.2015.368](https://doi.org/10.1109/ICCV.2015.368).
- [34] M. Zolfaghari, G. L. Oliveira, N. Sedaghat, and T. Brox, “Chained multi-stream networks exploiting pose, motion, and appearance for action classification and detection,” in *Proceedings of the IEEE International Conference on Computer Vision (ICCV)*, 2017.
- [35] V. Choutas, P. Weinzaepfel, J. Revaud, and C. Schmid, “Potion: Pose motion representation for action recognition,” Jun. 2018, pp. 7024–7033. DOI: [10.1109/CVPR.2018.00734](https://doi.org/10.1109/CVPR.2018.00734).
- [36] A. Shah, S. Mishra, A. Bansal, J.-C. Chen, R. Chellappa, and A. Shrivastava, “Pose and joint-aware action recognition,” in *Proceedings of the IEEE/CVF Winter Conference on Applications of Computer Vision (WACV)*, 2022, pp. 3850–3860.
- [37] A. Yan, Y. Wang, Z. Li, and Y. Qiao, “Pa3d: Pose-action 3d machine for video recognition,” in *2019 IEEE/CVF Conference on Computer Vision and Pattern Recognition (CVPR)*, 2019, pp. 7914–7923. DOI: [10.1109/CVPR.2019.00811](https://doi.org/10.1109/CVPR.2019.00811).
- [38] D. Ludl, T. Gulde, and C. Curio, “Simple yet efficient real-time pose-based action recognition,” in *2019 IEEE Intelligent Transportation Systems Conference (ITSC)*, 2019, pp. 581–588. DOI: [10.1109/ITSC.2019.8917128](https://doi.org/10.1109/ITSC.2019.8917128).
- [39] F. Yang, Y. Wu, S. Sakti, and S. Nakamura, “Make skeleton-based action recognition model smaller, faster and better,” in *Proceedings of the ACM Multimedia Asia*, ser. MMAsia ’19, Beijing, China: Association for Computing Machinery, 2020, ISBN: 9781450368414. DOI: [10.1145/3338533.3366569](https://doi.org/10.1145/3338533.3366569). [Online]. Available: <https://doi.org/10.1145/3338533.3366569>.

- [40] S. Asghari-Esfeden, M. Sznaier, and O. Camps, "Dynamic motion representation for human action recognition," in *2020 IEEE Winter Conference on Applications of Computer Vision (WACV)*, 2020, pp. 546–555. DOI: [10.1109/WACV45572.2020.9093500](https://doi.org/10.1109/WACV45572.2020.9093500).
- [41] P. Weinzaepfel and G. Rogez, *Mimetics: Towards understanding human actions out of context*, 2021. arXiv: [1912.07249 \[cs.CV\]](https://arxiv.org/abs/1912.07249).
- [42] W. McNally, A. Wong, and J. McPhee, *Star-net: Action recognition using spatio-temporal activation reprojection*, 2019. arXiv: [1902.10024 \[cs.CV\]](https://arxiv.org/abs/1902.10024).